# Pennsylvania State University

# Annual Progress Report: 2012 Formula Grant

**Reporting Period**

July 1, 2013 – June 30, 2014

**Formula Grant Overview**

The Pennsylvania State University received $6,589,749 in formula funds for the grant award period January 1, 2013 through December 31, 2016. Accomplishments for the reporting period are described below.

**Research Project 1: Project Title and Purpose**

*Targeting Pancreatic Cancer with Aptamers to the CCK-B Receptor* – The purpose of this research project is to select and develop aptamers which will be useful for specifically targeting pancreatic cancer; the aptamers will be selected to specifically recognize the CCK-B receptor, a growth-stimulatory receptor whose ligand is gastrin. Here we will explore targeting nanoliposomes to pancreatic cancer cells using high affinity aptamers; aptamer-targeted nanoliposomes will be developed containing reagents for imaging, or containing therapeutic reagents (chemotherapeutics, siRNAs, etc.)..

**Anticipated Duration of Project**

3/1/2013 – 9/30/2014

**Project Overview**

Recent advances in cancer therapy have come from understanding the biology or genetic make-up of a particular cancer. When these factors are identified, treatments can then be 'personalized' with more specificity by targeting of cancer-related receptors. One problem has been in developing an agent to selectively target nanoparticles, and their cargo, to facilitate nanoparticle up-take and delivery. G- protein coupled receptors (GPCRs) play a critical role in mediation of growth of gastrointestinal cancers. We have identified a receptor on pancreatic cancer, the CCK-B receptor, which is over-expressed in cancer compared to normal tissues and is responsible for growth stimulation. Our research team has shown that gastrin stimulates growth of pancreatic cancer through this GPCR. We have begun a collaboration to identify and characterize DNA aptamers that bind to the CCK-B receptor. DNA aptamers are highly structured oligonucleotides that bind with affinities comparable to or better than antibodies, are more stable in the peripheral blood than peptides or proteins, and are not immunogenic. Using a technique called Systematic Evolution of Ligands by Exponential Enrichment (SELEX) we have identified DNA aptamers that bind to the external gastrin binding site of the CCK-B receptor. This project will characterize aptamer affinity and specificity for the CCK-B receptor, and will use them to target nanoparticles

to pancreatic cancer cells *in vitro* and *in vivo*.

*We hypothesize that DNA aptamers that bind to the CCK-B receptor can be used to specifically target nanoliposomes to pancreatic cancer cells and can assist in delivering cargos such as siRNA or chemotherapeutics to pancreatic tumors*. In order to test this hypothesis we propose to: 1) Characterize the binding affinities and specificity of DNA aptamers to the CCK-B receptor, and 2) Study the efficacy of aptamers to target pancreatic cancer cells both in culture and in mice with pancreatic cancer. CCK-BR targeted nanoparticles could have a major use for delivering therapeutics as well as imaging agents.

**Principal Investigator**

Gary A. Clawson, PhD, MD
Professor
Pennsylvania State University
Hershey Medical Center
500 University Drive
Hershey, PA 17033

**Other Participating Researchers**

Gail L. Matters, PhD – employed by Pennsylvania State University

**Expected Research Outcomes and Benefits**

We expect to use Systematic Evolution of Ligands by Exponential Enrichment (SELEX) to identify aptamers with high affinities to the extracellular domain of the CCK-B receptor, which is highly expressed and selective for pancreatic cancer cells. These aptamers will be covalently attached to nanoliposomes, which will be packaged with either imaging reagents or therapeutics (chemotherapeutics, siRNAs, etc.), with the goal of specifically delivering them to pancreatic cancer cells in vivo.

**Summary of Research Completed**

*Aim 1) Characterize the binding affinities and specificity of DNA aptamers to the CCK-BR.*
Aim 1A: Identify aptamers which bind to the CCK-BR.
The aptamer (AP) selection protocol which yielded the AP family including PXT733 did not produce suitable results for binding CCKB-R on intact cells for flow cytometry. We therefore modified our selection protocol, and in addition also decided to select for 2 extracellular CCKB-R regions, the original BR5-21 aa region, as well as BR40-57. The modified selection was performed for 14 rounds. For the 1st round a full-length library (81 nt, including fixed primers) was used, and from the 2nd round onward the selections used the random region with the 3'-fixed region (66 nt) but without the 19 nt 5'-fixed region (this was done because removal of both fixed-primer regions didn't work for cell binding for unknown reasons). For the first 6 rounds, independent selections for the BR5-21aa or 40-57 aa regions were performed including rounds with PANC-1 cells. Each round was performed with sequential binding to: glass beads only

(background) – glass bead with specific BR peptide – Cos-1 cells (negative for CCKB-R), where the unbound fraction was harvested – PANC-1 cells (positive for CCKB-R). For the final 4 rounds, 2 step selections were performed, using the Cos-1 and PANC-1 cells. We then cloned ~ 100 APs from this "14.2" selected pool. 93 sequences were analyzed, and aligned using Clustal software (Figure 1a).

After sequence alignments, each individual sequence was further analyzed by single strand count, and based on the subgroups defined by alignment, ss-counts, structure, and predicted minimal free energies, 25 aptamers were selected, 14 selected for binding to the BR5-21 region, and 11 for binding to the BR40-57 region. 4 APs from each group were selected for further initial testing (2 representative mFold predicted structures are shown in Figure1b). These APs showed Kd in the 15 pM range (Figure 1c).

Based on both peptide and cell-based selection data, a panel of eight CCK-BR aptamers were identified for further analysis. These CCK-B receptor selected aptamers demonstrated an average Kd in the pM range, which is 10-100 times better than that of gastrin (approximately 1nM.

Although the average length of the selected aptamers was 46-66 nucleotides, there was no strong sequence homology among aptamers that would indicate a unique CCK-BR binding motif (see Figure 1b).

<u>Aim 1B: Determine whether the identified aptamers antagonize gastrin signaling.</u>
There was no significant competition for AP binding by the CCKB-R small molecule antagonist YM022, making it very likely that APs will not trigger gastrin signaling.

*Aim 2) Study the efficacy of aptamers to target pancreatic cancer cells both in culture and in mice with pancreatic cancer.*
<u>Aim 2A:Encapsulation of cargo molecules and attachment of aptamers to nanoliposomes (NLs)</u>.

Formulation of pegylated, ceramide-containing anionic NLs (pcaNLs): pcaNLs are synthesized in the Penn State Nanoliposome Core Facility and all lipids are purchased from Avanti Polar Lipids (Alabaster, AL). The components of the pcaNLs are prepared from chloroform-solubilized lipids. The molar ratios, optimized for delivery to PDAC cells in vitro, are 3.75 DSPC: 1.75 DOPE: 0.5 PEG(2000)-DSPE: 0.5 PEG(750)-C8-ceramide: 1 DHDP: 3 C6-ceramide. DSPC is (1,2-Dioleoyl-sn-glycero-3-phosphocholine); DOPE is (1,2-Dioleoyl-sn-Glycero-3-Phosphoethanolamine); PEG(2000)-DSPE is (1,2-distearoyl-sn-glycero-3-phosphoethanolamine-N-[methoxy(polyethylene glycol)-2000]); PEG(750)-C8 ceramide is (N-octanoyl-sphingosine-1-[succinyl(methoxy polyethylene glycol)-750]; DHDP is (dihexadecyl phosphate); C6-ceramide is (M-hexanoyl-D-erythro-sphingosine)(3.75:1.75:0.5:0.5:1:3). This yields PcaNLs with 28.5 molar% C6 ceramide, 9.5 molar% PEGylated shell, and 9.5 molar% anionic DHDP, which facilitates encapsulation of active compounds in the void volume of the pcaNLs (we can get encapsulation efficiencies of nearly 80%; without inclusion of anionic constituents in the pcaNLs, efficiencies of encapsulation can be below 10% and the resulting NLs are unstable).

We used TCSPC (time-correlated single photon counting)-based FCS (Fluorescence correlation spectroscopy) measurements to determine NL size and number in solution. Fluorescence correlation spectroscopy (FCS): TCSPC contains photon arrival times relative to the laser pulse and to the start of the experiment. From these arrival times we can calculate a temporal autocorrelation function which can be fit by the equation: $G(\tau)=(1/Np)*(1/(1+\tau/\tau D)*1/(1+\tau/\kappa \tau D)^{0.5}$ where Np is the number of particles in the focal volume (<10), $\tau$ is the correlation time, $\kappa$ is the ratio of height to radius of the focal volume, and $\tau D$ is the characteristic diffusion time. Np and $\tau D$ are the critical readouts from FCS as they provide precise concentration of particles and size of the particles, respectively. Size is calculated from $Rh=4kBT* \tau D /(6\pi\eta\omega 2)$ where Rh is the hydrodynamic particle radius. kB is Boltzmann's constant, T is temperature, and $\eta$ is solvent viscosity. Such data is indispensable for calculating encapsulation efficiency and for preventing free dye from eliciting drug side effects. Since particle size is directly relevant for uptake efficiency by cells, this measurement also could become part of the comprehensive particle characterization strategy. This gives us the concentration of NLs in solution. For our quantitation experiments, particle counts were ~ $6x10^{15}$. We also can estimate pcaNL size by dynamic light scattering. Zeta potential is measured to determine overall pcaNL charge.

Aliquots of AP-conjugated pcaNLs were then enzymatically labeled at their 5' ends with 32P-ATP using polynucleotide kinase. We used 10 pm of gamma-32-ATP in a 40 ul reaction, and then reactions were filtered through filters with an exclusion cutoff of 30kDa (which traps the free APs used for the quantitation curve), and 32P-incorporated was measured. These data were then used to determine that ~ 75 APs were incorporated for the surface area for 80 nm diameter pcaNLs.

The next step was coupling of the selected APs to nanoliposomes (NLs). The full length (66 nt) and short (45 nt, representing the random region with the fixed primer regions removed) versions of a selected AP (PXT1153) were synthesized with a 3'-C6-NH2 moiety, which allows for facile coupling to PEG using the primary NH2 group. This modification was unlikely to alter AP binding parameters, since the fixed 3'-region was left attached during the selection, and mFOLD modeling shows that the 3'-end of all selected Aps are in unstructured regions. Both the long and short form of the modified APs were rechecked for binding; no change in binding parameters was observed. In additional studies, we will verify that the APs do not activate gastrin signaling pathways (this is unlikely given the regions selected), and in our ongoing R21 we will explore potential competitive inhibition, etc. We will also perform studies using AP-PcaNLs (conjugated AP as 3'-NH2-C6-aptamer) to verify that degradation of the AP does not occur in plasma. The 3'-terminus of the modified AP will be conjugated and thus not exposed. However, if for any reason we need to couple it using the 5'-terminus, we have previously shown that addition of 5'-inverted Ts to the 3' end of APs renders them stable in media (10% serum) for > 24 h, and we would therefore add an inverted 5'T to the 3'-end.

The modified long or short versions of PXT1153 AP were then covalently coupled to pegylated C6-ceramide containing anionic nanoliposomes (pcaNLs). Following coupling, particle numbers were determined spectrometrically.

Aim 2B. Evaluate the ability of CCK-BR aptamers to improve cellular up-take of loaded NLs *in vitro*.
With 32P-APs selected from Aim 1, these showed 8-12X improved binding to PANC-1 cells vs. Cos-1 cells, although these measurements almost certainly underestimate the true selectivity, due to artefactually high 32P backgrounds.

In pancreatic ductal adenocarcinoma (PDAC) cell uptake experiments (Figure 2), we found high selectivity for the initial AP tested (PXT1153) for PANC-1 cells (high CCKBR expression) vs. BxcPC-3 (low CCKBR expression).

We also measured FITC-AP uptake on PANC-1 clones which were engineered to over-express the CCKB-R or which had the CCKB-R permanently knocked down. The extent of AP uptake closely paralleled expression levels of CCKB-R (Figure 3), and there was no significant competition for AP binding by the CCKB-R small molecule antagonist YM022. As additional controls, untreated or vehicle treated PANC-1 cells showed no FITC- fluorescence, and PANC-1 cells treated with a non-selected, FITC-labelled aptamer (PXT 38) also showed no aptamer up-take (Figure 3). BxPC-3 cells, with lower levels of CCKB-R expression, also showed reduced PXT 1153 up-take (data not shown). This work completed Milestone 1, which was to complete *in vitro* and cell-based aptamer selection/characterization.

These pcaNLs, conjugated with APs targeting the CCKB-R, are currently being tested in PANC-1 cells in culture, and they will be tested for in vivo targeting. Our earlier work demonstrated that calcium phosphosilicate composite nanoparticles were successfully targeted to xenografts of pancreatic cancers cells in vivo, when gastrin was used as a targeting moiety and the nanoparticles were loaded with indocyanine green (ICG). Since our CCKB-R-targeted APs have 1000X greater affinity for the CCKB-R than gastrin, we anticipate improved localization. We used Rhodamine WT for cellular uptake studies; these studies have just been completed,

Aim 2C: Aptamers that enhance NL up-take *in vitro* will be tested for their ability to target NL up-take by orthotopic human pancreatic tumors *in vivo*.
No work was done on this Aim during the reporting period.

Figure 1. Results of Aptamer Selection against extracellular CCKB-R aa regions 5-21 and 40-57**.** 14 multi-step rounds of selection were performed as described; 100 APs from the pools were cloned and sequenced and aligned using Clustal (Panel a simply shows the "family tree"). Representative APs (25) from various groups were chosen and from various analyses, 8 APs (4 from each group) were chosen for further study. Panel b shows mFold predicted structures for 2 representative APs. Free energy calculations showed stable predicted secondary structures, with ΔG's ~ -8 Kcal/mol. Binding experiments disclosed Kd's in the 10 pM range (Panel c shows a binding experiment with PXT1153, which had a Kd = 15 pM).

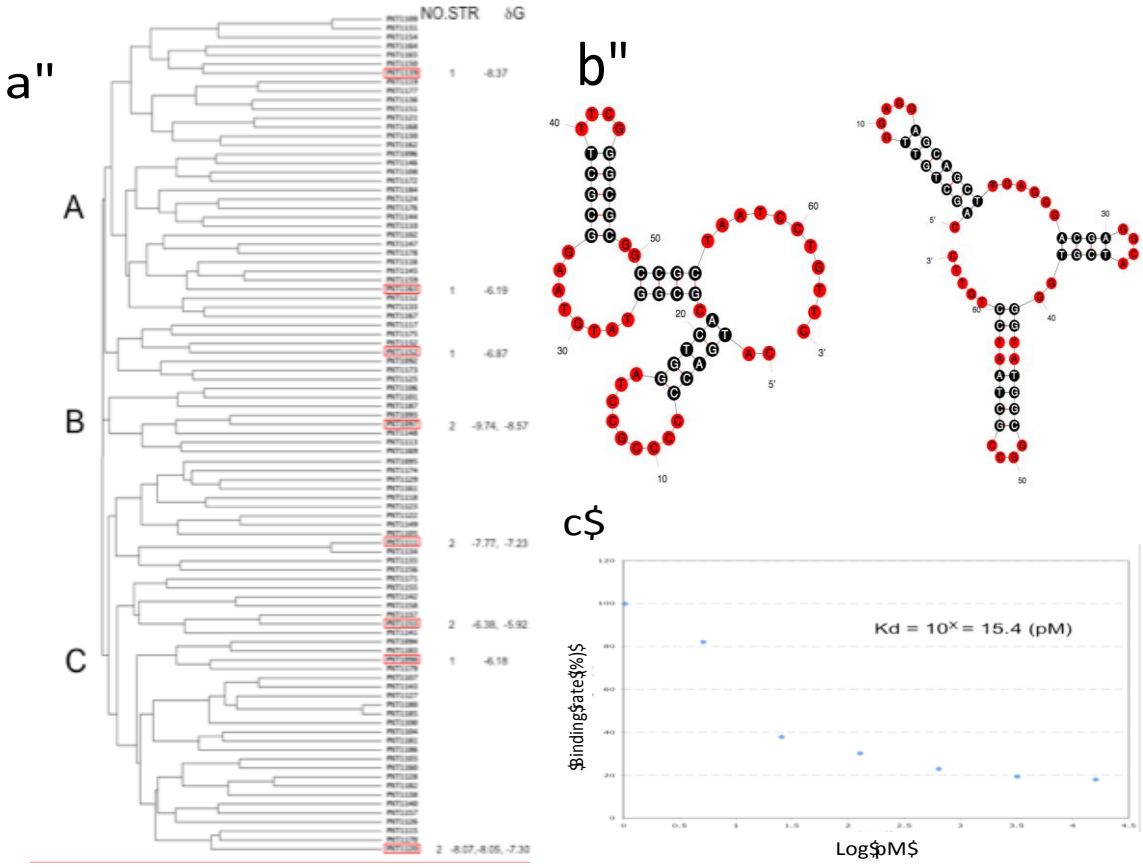

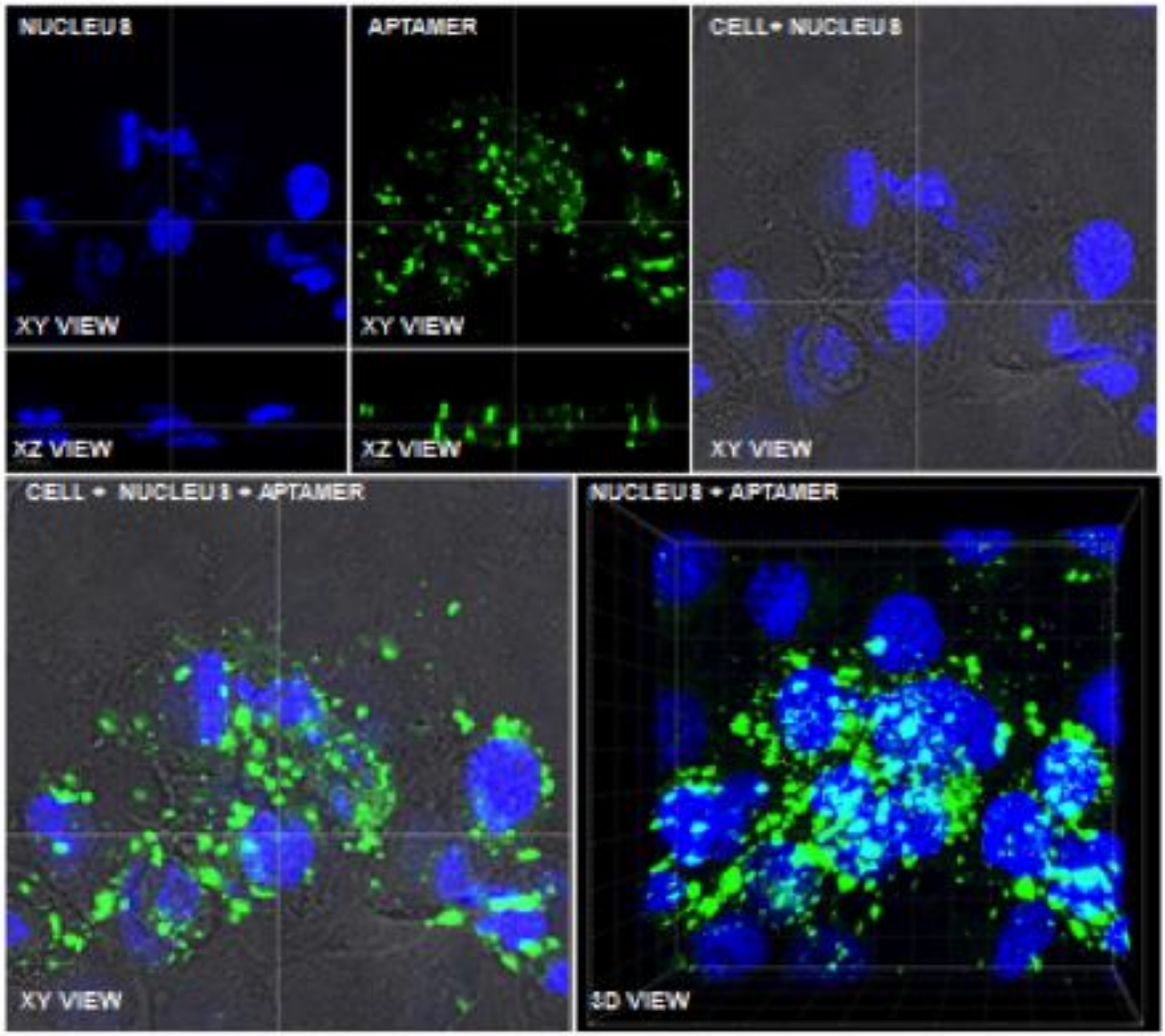


Figure 2. Confocal images of up-take of aptamer PXT1153 (FITC-labeled, green) by CCKBR-expressing PANC-1 cells. Intracellular aptamer distribution is indicated relative to the nuclei (blue) and other cell features (gray, bright field image, lower left). CCKB-R overexpressing PANC-1 cells were incubated with the FITC-aptamer for 24 hours, fixed, counterstained with Hoechst 33342 nuclear stain, mounted on slides using ProFade Gold mounting medium and imaged on Leica SP8 Confocal microscope.

Figure 3. Uptake of Fluorescently-labeled AP (PXT1153) by PDAC Cell lines. Bars (left to right): Panc-1 Wild type; PANC-1 WT +YM022 (a CCKB-R antagonist); PANC-1 CL14 (a clone engineered to overexpress CCKB-R; PANC-1 CL14 + YM022; PANC-1 CL14 treated with a non-specific control AP (PXT38); PANC-1 CL42 (a clone with knockdown f CCKB-R expression); PANC-1 CL42 + YM022.

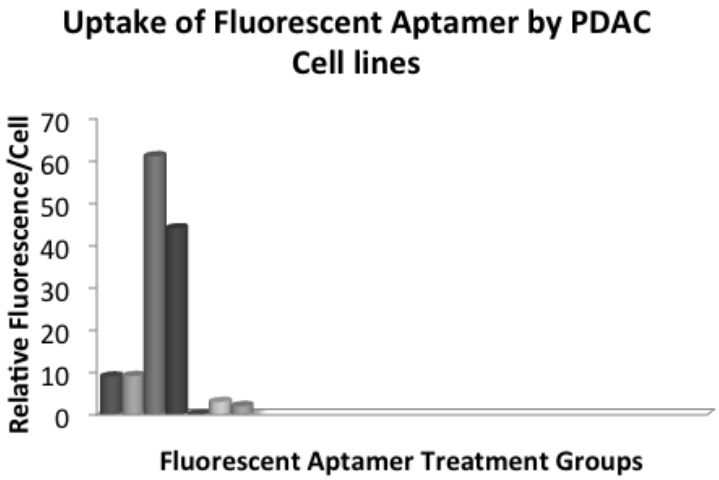


## Research Project 2: Project Title and Purpose

*Perioperative Circulating Tumor Cell Detection in Stage IV Colorectal Cancer* – Circulating tumor cell (CTC) isolation during colorectal cancer (CRC) liver and lung metastasectomy will increase understanding of CTC shedding during surgery, discover targets for guided therapy and identify high-risk patients for recurrence. This study will also evaluate a novel filtration-based technology that allows isolation of viable cells. By analyzing biomarker expression in CTCs, therapeutic molecular targets can potentially be identified. The studies to sample CTCs intraoperatively apply innovative approaches to unsolved problems in patients with metastases from CRC. The results can be fundamentally important to understanding cancer spread, and further personalize therapy in patients undergoing cancer-related surgery.

### Anticipated Duration of Project

1/1/2013 – 12/31/2016

### Project Overview

The overall hypothesis is that circulating tumor cells (CTCs) can be enriched during CRC liver and lung metastasectomy, and these CTCs can cause recurrences and express molecular targets for intervention. The objective of the project is that CTC isolation during metastasectomy will increase understanding of CTC shedding during surgery, discover targets for molecular guided therapy and identify patients who are at high-risk for recurrence and would benefit from additional treatments. In a pilot clinical study over 24 recruitment months, 40 patients with

resectable CRC liver (n=30) and lung (n=10) metastases will be prospectively recruited for perioperative CTC isolation.

*Specific Aim I: CTCs will be quantified in multiple blood compartments during CRC liver and lung metastasectomy.* Perioperatively, blood will be collected directly before, during and after metastasectomy from the radial artery (liver inflow and lung outflow), a central venous line in the right atrium (proximal liver outflow and lung inflow), and a peripheral venous line (distal lung inflow). Blood will be processed with the FDA-approved CellSearch system and the novel FMSA device.

*Sub-Aim Ia: Determine the effect of surgical ligation of the tumor blood inflow vs. outflow on CTC shedding.* We hypothesize that surgical ligation techniques induces CTC dissemination and cause early recurrences. Both the liver and lung will be studied, comparing two organs with different vascular anatomy and applied surgical techniques. Our protocol allows comparing how CTC numbers behave with initial ligation of the metastases inflow (liver) and outflow (lung), respectively.

*Sub-Aim Ib: Cancer stem cell and key signaling/proliferation biomarkers will be analyzed.* We hypothesize that CTCs overexpress cancer stem cell molecules and poor prognostic markers. Biomarker analysis will identify therapeutic targets and markers for disease monitoring. CTCs will be immunostained with a multiplex protocol using quantum dots (QD®) against CEA, CD133, pERK, pAKT, Ki67 and EGFR.

*Specific Aim II: Perioperative CTC counts will be correlated with cancer recurrences.* We hypothesize that high perioperative CTC counts correlate to recurrences after surgery. CTC numbers will also be determined every 3 months after surgery, and correlated to recurrences/survival.

**Principal Investigator**

Wafik El-Deiry, MD, PhD
Professor
The Pennsylvania State University
College of Medicine
500 University Drive, H070
Hershey, PA 17033-0850

**Other Participating Researchers**

Siyang Zheng, PhD – employed by The Pennsylvania State University

**Expected Research Outcomes and Benefits**

Findings on perioperatively detected CTCs have the potential to specify selection criteria for patients who will benefit from CRC liver and/or lung metastasectomy or other treatments based on perioperative CTC numbers. The study will improve CTC isolation efficiency and identify the

compartment of most clinical significance for future CRC staging and chemosensitivity testing. CTC sampling in direct proximity to the metastases could be easily added, as transjugular hepatic vein (outflow of liver) and radial artery (outflow of lung) blood samplings are both routine clinical procedures. Both CRC liver and lung metastases will be studied, comparing two organs with divergent surgical techniques that have to be applied by the surgeon. If CTC dissemination occurs after ligation of the inflow, current surgical practice will need to be questioned and vascular ligation should be performed either inversely or simultaneously to prevent intraoperative spread. This study will evaluate a novel filtration-based technology, the Flexible Micro Spring Array (FMSA) device. Preliminary data has shown that the FMSA device has a higher intraoperative CTC capture efficiency, and it allows isolation of viable cells for further testing with implications for personalized treatments. The FMSA also allows bedside CTC isolation at low cost. By analyzing biomarker expression in CTCs and metastases there is potential for identification of therapeutic molecular targets. The project applies innovative approaches and novel technologies to unsolved problems in patients with metastases of CRC. This is a prospective pilot study that has the limitation of low sample size (that can be increased in future studies). The results can be fundamentally important to understanding cancer spread, and further personalize therapy in patients undergoing cancer-related surgery.

**Summary of Research Completed**

During the last few months of work on this project there have been some changes. Dr. Kaifi left the institution and Dr. El-Deiry took charge of leading the project. Dr. El-Deiry was previously involved in conceptualizing the project and in mentoring Dr. Kaifi in achieving its goals. Another change that has occurred over the last several months is that there has been a shortage of FMSA devices that have been available for this project from a collaborator (Dr. Siyang Zheng). As such the research team has turned its attention to using a commercial source for a filter device to isolate and characterize circulating tumor cells. This has been going well in terms of showing feasibility and yield of isolation as well as the ability to detect molecular markers within isolated patient-derived circulating tumor cells. There have been ongoing efforts to work with Drs. Gusani, Wong, and Soybel in the Department of Surgery in order to plan to fulfill the translational goals that involve intra-operative sampling. There have been discussions regarding further refining the goals of intra-operative sampling in order to maximize yield of scientific knowledge that is relevant to the tumor biology as well as to gain insights regarding how intraoperative sampling that may in the future involve sampling through interventional radiology procedures, and may impact on the care of patients with circulating tumor cells. Such impact is envisioned in the decision making as far as surgical technique and there may be impact regarding whether some patients may be offered neoadjuvant or adjuvant therapies based on the intraoperative sampling.

*Specific Aim I: CTCs will be quantified in multiple blood compartments during CRC liver and lung metastasectomy.*

CTCs were quantified with both CellSearch system and FMSA device in multiple blood compartments during CRC liver and lung metastasectomy. Blind comparative detection by the CellSearch system and the FMSA device of CTCs enriched from equivalent 7.5-mL clinical samples, at least 1 CTC in approximately 76% of clinical samples was detected by the FMSA

device as opposed to 1 in approximately 22% by CellSearch system. CTC staining images from FMSA devices are shown in Figure 1.

There has been a shortage of FMSA devices that have been available for this project from a collaborator. As such the research team has turned attention to using a commercial source for a filter device to isolate and characterize circulating tumor cells. This has been going well in terms of showing feasibility and yield of isolation as well as the ability to detect molecular markers within isolated patient-derived circulating tumor cells. The recovery rate of CTCs with CellSieve microfilters is 85~98%. CTC staining images from CellSieve microfilters are shown in Figure 2.

*Sub-Aim Ia: Determine the effect of surgical ligation of the tumor blood inflow vs. outflow on CTC shedding*

There have been efforts to work with Drs. Gusani, Wong, and Soybel in the Department of Surgery in order to plan to fulfill the translational goals that involve intra-operative sampling. There have been discussions regarding further refining the goals of intra-operative sampling in order to maximize yield of scientific knowledge that is relevant to the tumor biology as well as to gain insights regarding how intraoperative sampling that may in the future even involve sampling through interventional radiology procedures, may impact on the care of patients with circulating tumor cells. Such impact is envisioned in the decision making as far as surgical technique and there may be impact regarding whether some patients may be offered neoadjuvant or adjuvant therapies based on the intraoperative sampling.

*Sub-Aim Ib: Cancer stem cell and key signaling/proliferation biomarkers will be analyzed*

Cancer proliferation biomarkers pERK, pSTAT3 and anti-apoptotic Mcl-1 are analyzed. Immunostaining of cancer cells shows pERK, pSTAT3 and Mcl-1 are overexpressed as shown in figure 3.

*Specific Aim II: Perioperative CTC counts will be correlated with cancer recurrences.*

No work was done on this aim during the reporting period.

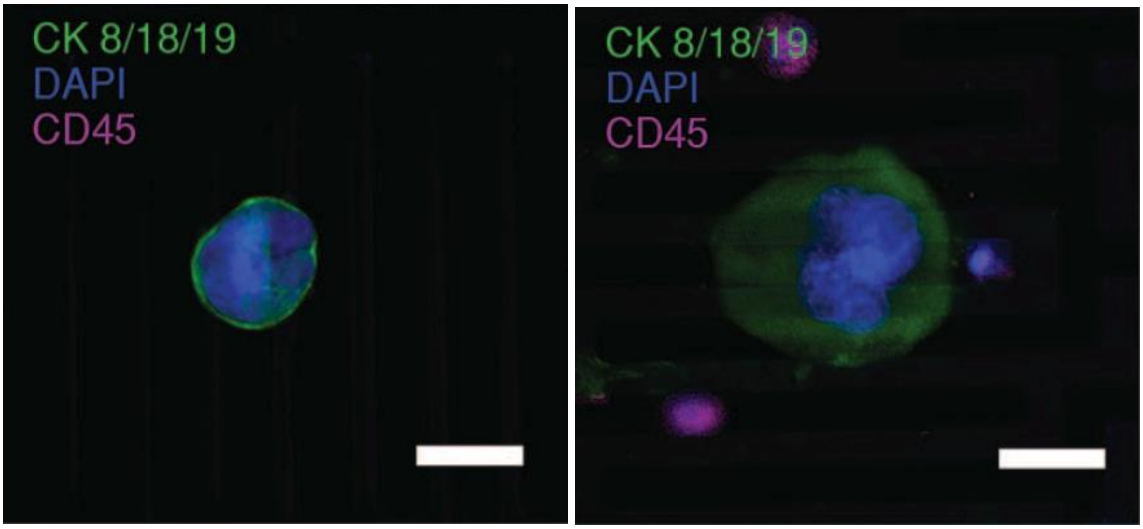


Figure 1

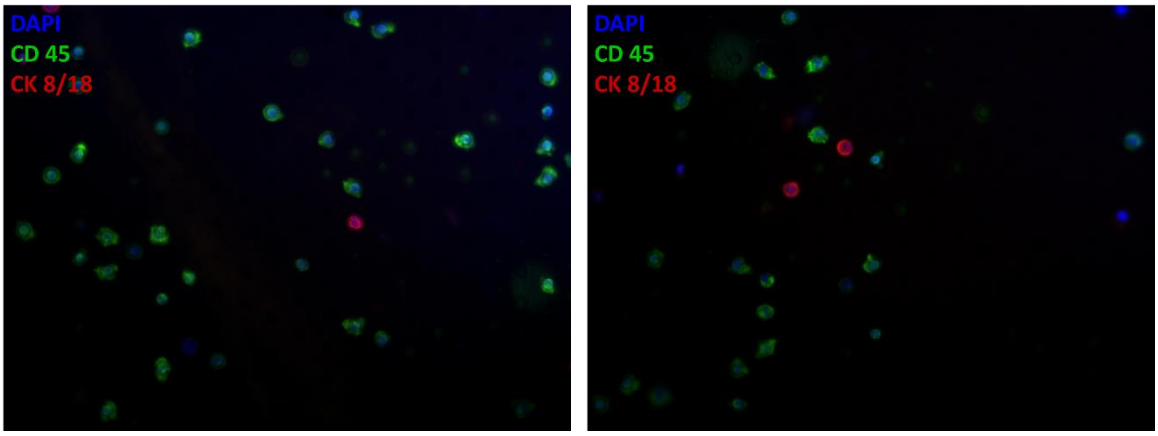


Figure 2

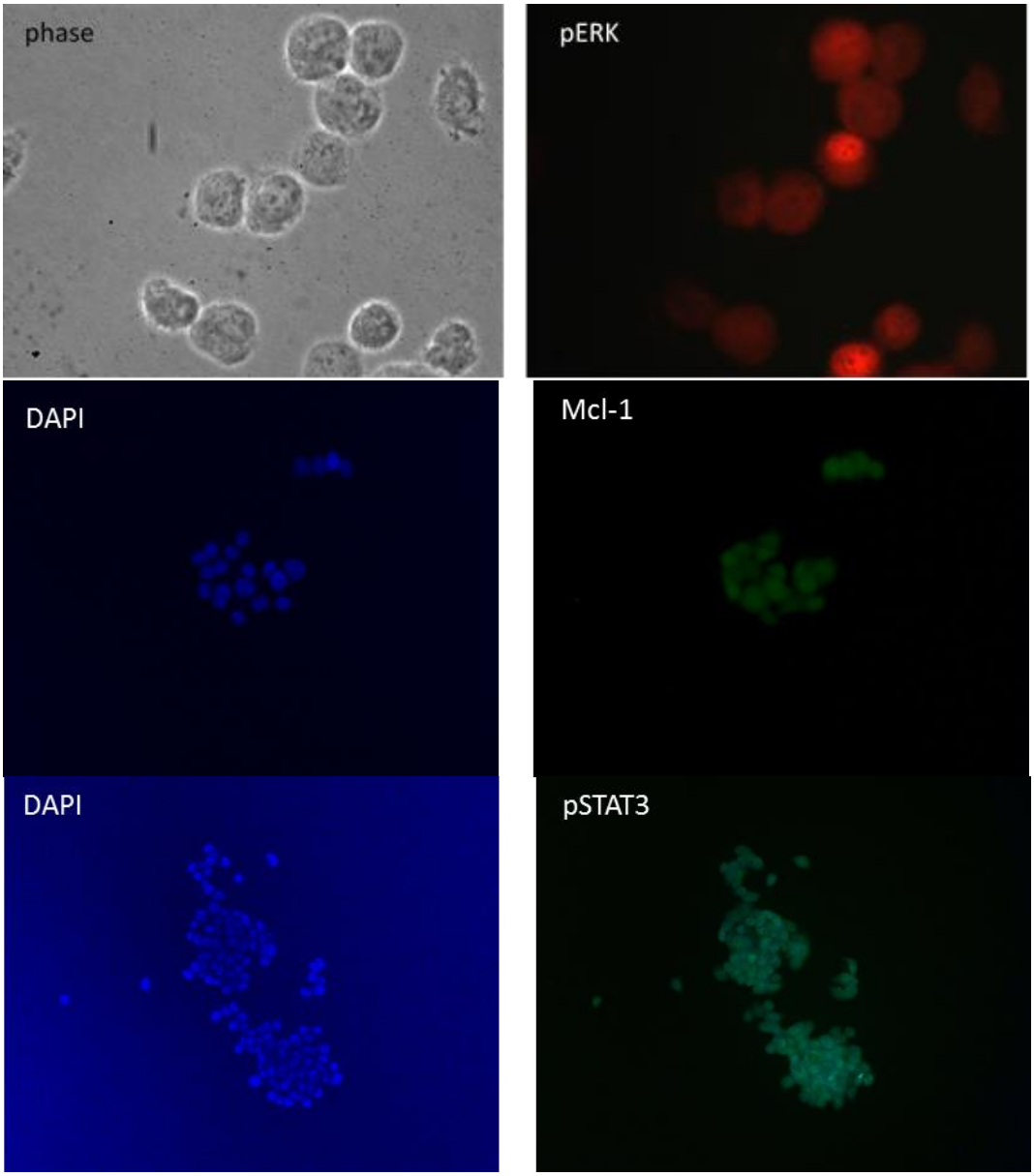


Figure 3

**Research Project 3: Project Title and Purpose**

*Analysis of the Role of YAP1 in the Self Renewal of Leukemia Stem Cells* – Leukemia is a hierarchical disease with Leukemia stem cells occupying the apex. Conventional therapies for leukemia are designed to kill leukemia cells, but leukemia stem cells have active mechanisms to evade these drugs. Leukemia stem cells that survive treatment can then cause relapse of disease. Thus, a greater understanding of the mechanisms that regulate the self renewal of leukemia stem cells will identify new targets for therapeutic intervention. The purpose of this project is to test the hypothesis that Yap1 promotes the self renewal of leukemia stem cells and will test whether

inhibiting Yap1 can eliminate leukemia stem cells and effectively treat disease. These studies are initial basic studies using mouse models of leukemia that if successful could be translated into the clinic.

**Anticipated Duration of Project**

6/1/2013 – 12/31/2014

**Project Overview**

Leukemia is a hierarchical disease where a small population of leukemia stem cells (LSCs) is responsible for the generation of bulk leukemia cells. LSCs pose a significant problem for the treatment of leukemia in that they are in general resistant to conventional chemotherapy, which leads to post treatment relapse of the disease. The focus of this project is to identify common mechanisms that regulate LSC self renewal as a means of targeting LSCs, which would improve the efficacy of conventional treatment and lead to improved therapies. The primary hypothesis of this project is that the decision between self renewal and differentiation relies on the antagonism between two signaling pathways. p53 promotes the differentiation of LSCs, while Yap1 promotes self renewal.

The first aim of this project seeks to firmly establish the role for the Yap1-p53 axis in regulating LSC self renewal using both a murine model of Chronic myelogenous leukemia (CML) and a murine model of Acute myeloid leukemia (AML). The experiments outlined in this aim are designed to demonstrate three outcomes: (i) Using a conditional allele of Yap1, show that deletion of Yap1 in CML blocks the self renewal of LSCs, while knockdown of p53 expression increases LSC self renewal; (ii) Demonstrate that in a murine model of AML, MLL-AF9 expression down-regulates p53 expression and increases Yap1 expression, which drives the self-renewal of LSCs; (iii) Demonstrate that deletion of Yap1 in AML LSCs decreases LSC self renewal, while knockdown of p53 increases self renewal. These three goals will establish that the Yap1-p53 axis is a common regulator of LSC self renewal in myeloid leukemia. The impact of this work is great in that it will identify a common signaling pathway that could be targeted to treat diverse myeloid leukemias.

The second aim, to establish a role for Sphingosine 1- phosphate (S1P) in regulating Yap1 in CML and AML LSCs, proposes to expand previous work we have done. We have tested a sphingosine kinase 1 (Spk1) inhibitor (SKI178). SKI178 was very effective in treating murine MLL-AF9 leukemia. Recently, others showed that sphingosine-1-phosphate, the product of Spk1 increased Yap1 activity by promoting nuclear localization of Yap1. The expectation from the experiments outlined in Aim2 is that SKI178 inhibits the nuclear localization of Yap1, which in turn leads to increased p53 activity and loss of LSC self renewal. We will test this hypothesis in both the CML and the AML models. This aim builds on the findings of Aim1 and identifies a therapeutic target and a potential therapy that blocks Yap1 dependent self renewal of LSCs.

## Principal Investigator

Robert F. Paulson, PhD
Professor of Veterinary and Biomedical Sciences
Pennsylvania State University
115 Henning Building
University Park, PA 16802

## Other Participating Researchers

Shailaja Hegde, BS – employed by Pennsylvania State University

## Expected Research Outcomes and Benefits

The expected outcomes of this research are two-fold. First, we will investigate the basic mechanisms that regulate the self renewal of leukemia stem cells. Inhibition of self renewal blocks the ability of leukemia stem cells to maintain disease and therefore represents a potential new therapy for leukemia. We have identified a potential regulatory network that promotes Leukemia stem cell self renewal and the experiments outlined here will establish a role for the p53-Yap1 signaling axis in this process. Our hypothesis is that this signaling pathway is a common pathway for regulating self renewal in both chronic myelogenous leukemia and acute myeloid leukemia, which if true would allow for the development of a common therapy that could be used to treat both diseases. Second, we will build on previous work from my lab that shows that inhibiting sphingosine kinase 1 (Spk1) blocks the progression of leukemia in a murine model of acute myeloid leukemia. We hypothesize that this inhibitor will affect the p53-Yap1 signaling pathway. These experiments will identify the mechanism by which inhibiting Spk1 blocks the progression of leukemia, which could hasten the development of this drug as a therapy for leukemia. The impact of this project is that it will increase our knowledge of the molecular mechanisms that regulate Leukemia stem cell self renewal that will identify new targets for therapeutic intervention.

## Summary of Research Completed

*Aim 1: establish the role for the Yap1-p53 axis in regulating LSC self renewal using both a murine model of Chronic myelogenous leukemia (CML) and a murine model of Acute myeloid leukemia (AML).*

Using a murine model for chronic myelogenous leukemia (CML) we have addressed the first objective of Aim1. Previous work in the lab identified a series of cell surface markers that allowed us to isolate and culture CML LSCs. Using serial replating assays we can measure self-renewal in vitro, in addition we can transplant cells into mice where they cause disease. Based on our previous work we have developed a model for the self renewal of LSCs in CML that relies on the ability of LSCs to interact with signals in their microenvironment. Our model proposes that hedgehog (HH) signaling functions to reduce p53 activity and reduced p53 activity leads to the expression Yap1. Yap1 has been implicated in stem cell self renewal in ES cells and cancer stem cells (figure 1). We tested the effects of manipulating p53 or Yap1 expression on the ability

of LSCs to self-renew in vitro and cause disease in vivo. We would predict that decreasing Yap1 expression would decrease the number of LSCs and prevent the progression of disease, while the converse would be true when p53 expression was decreased. Using short hairpin RNAs (shRNAs) that target Yap1 (Yap1KD), we observed an approximately 70% knockdown of Yap1 expression. We tested Yap1 KD LSCs in both in vitro and in vivo assays. In vitro we assess LSC activity by their ability to form large compact colonies in methocel media containing Shh+GDF15+SCF+IL-3, which we refer to as LSC colonies. In contrast, non-LSC CML progenitors form granulocyte-macrophage colonies (CFU-GM) when plated in methocel containing only GM-CSF. Typically CML-LSC cultures contain mainly cells that form LSC colonies with few cells that form CFU-GM. When we tested CML-LSCs expressing a Yap1 shRNA (Yap1KD) we observed a significant decrease (15% of control) in LSC numbers in vitro. This decrease was accompanied with a significant increase in cells that form CFU-GM colonies. These data support the idea that a loss of Yap1 expression results in the loss of LSCs that leads to an increase in non-LSC CFU-GMs. To test the effects of Yap1KD in vivo, LSCs infected with the Yap1 shRNA virus or control scramble virus were transplanted into mice and the progression to CML was monitored by complete blood count and survival. Knock down of Yap1 expression translated into 100% survival of mice transplanted with Yap1KD LSCs. The mice transplanted with Yap1KD cells showed no sign of disease and did not exhibit elevated white blood cell (WBC) counts. These data support the hypothesis that Yap1 promotes self-renewal and inhibits LSCs from terminal differentiation (Figure 2).

In the converse experiments, we knocked down the expression of p53 using shRNA lentiviruses. Compared to scramble control viruses, knock down of p53 expression lead to a two fold increase in Yap 1 expression. In order to investigate the mechanism by which p53 regulates Yap1 expression, we first examined the Yap1 locus for putative p53 binding sites. Two sites that contained the p53 binding consensus sequence were identified in intron 4 of the Yap1 locus. These sites were conserved in multiple species and analysis of the regulatory potential by RP score suggested that they could be putative regulatory sites. We tested whether p53 was associated with these sites by Chromatin immunoprecipitation (ChIP) assay. CML LSCs were treated with Nutlin3 which stabilizes p53 protein. The data in figure 3B show that p53 antibodies can precipitate a chromatin fragment containing either the p53-1 or p53-2 site. In order to demonstrate that these sites could mediate p53 dependent regulation of Yap1, we cloned a fragment of the Yap1 locus that contained both sites upstream of firefly luciferase reporter gene. This construct was transfected in 293T cells along with a Renilla luciferase expression plasmid to control for transfection efficiency. Cells were treated $\pm$ Nutlin3 to activate p53 activity. In absence of nutlin3, cells transfected with the luciferase plasmid containing wild type p53 sites exhibited increased luciferase compared to a control plasmid that did not contain the Yap1 locus fragment. However after 12 hours of Nutlin3 treatment, the luciferase activity was significantly inhibited. Mutation of either site 1 or site or both decreased the basal luciferase activity in the absence of Nutlin 3, however after Nutlin3 treatment the luciferase activity of the mutants increased suggesting that mutation of these sites blocked the ability of p53 to repress the expression of luciferase. Based on these observations we conclude that p53 represses Yap1 expression by binding to the sites in intron 4 of the Yap1 locus. In addition to regulation at the level of expression, Yap1 is also regulated by subcellular localization. Yap1 is phosphorylated on serine 127, which makes a docking site for 14-3-3 sigma. This protein then promotes the shuttling of Yap1 out of the nucleus and into the cytoplasm where it is degraded. We analyzed

whether p53 activity could affect the expression of 14-3-3 sigma. We treated CML LSCs with Nutlin3 to induce p53 activity and tested whether this treatment could increase the expression of 14-3-3 sigma. In figure 3D, the data show that Nutlin3 treatment significantly increases the expression of 14-3-3 sigma. These data support a model where p53 acts directly to down regulate Yap1 expression and also affects the function of Yap1 protein by up-regulating the expression of 14-3-3 sigma, a negative regulator of Yap1 protein function (Figure 3).

*Aim 2: establish a role for Sphingosine 1- phosphate (S1P) in regulating Yap1 in CML and AML LSCs, proposes to expand previous work we have done.*

We also made progress on Aim2, which proposed to examine whether inhibition Sphingosine 1 Kinase (Spk1) by the chemical inhibitor Ski178 blocks the activity of Yap1 thereby leading to a loss of LSCs. Previous work included as preliminary data in the grant application showed that SKI-178 a Spk1 inhibitor was able to reduce leukemia and promote survival in a mouse model of AML. We tested whether inhibition of sphingosine kinase affected p53-Yap1 regulatory network control of LSC self-renewal (Figure 1). For these experiments we used both the murine model for CML and a murine model of acute myeloid leukemia (AML) caused by the MLL-AF9 fusion oncoprotein. We tested CML LSCs in the LSC/CFU-GM colony assay in the presence or absence of SKI-178. Treatment with SKI-178 significantly reduced the number of LSC colonies, while the number of CFU-GM increased (figure 4A). These data suggest that similar to inhibiting Yap1 expression, inhibition of Spk1 leads to a shift from LSC to non-LSC CFU-GM colony forming cells. We further investigated this effect by treating CML-LSCs with SKI-178 and then examining the expression of Yap1, p53 and 14-3-3 sigma at 12, 24, 48 and 72 hours of treatment. As predicted by our model, we observed a decrease in Yap1 expression which correlated with an increase in p53 and 14-3-3 sigma expression. These data support the colony assay data and suggest that inhibition of Spk1 by SKI-178 decreases LSC numbers by blocking Yap1 expression and promoting the 14-3-3 sigma mediated clearance of Yap1 from the nucleus. We extended these observations to a murine model of AML. AML LSCs were cultured in the presence of SKI-178. We measured Yap1 expression, p53 expression and 14-3-3 sigma expression over the same 72 hour time course. Similar to what we observed with CML LSCs, treatment with SKI-178 lead to the down regulation of Yap1 expression which was correlated with the increase in p53 and to a lesser extent 14-3-3 sigma expression. These are consistent with a model where Sphingosine -1- phosphate promotes the self-renewal of LSCs. Blocking Spk1 leads to a decrease in LSCs caused by a loss of Yap1 expression and an increase in p53 expression (Figure 4).

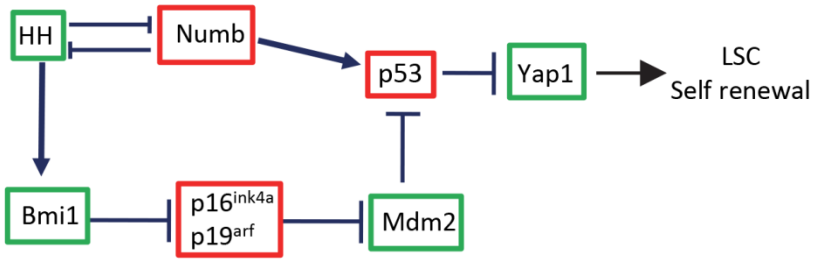


Figure 1. Overall model for regulation of LSC self-renewal in CML. Green boxes represent signals that promote self renewal, red boxes represent signals that inhibit self renewal..

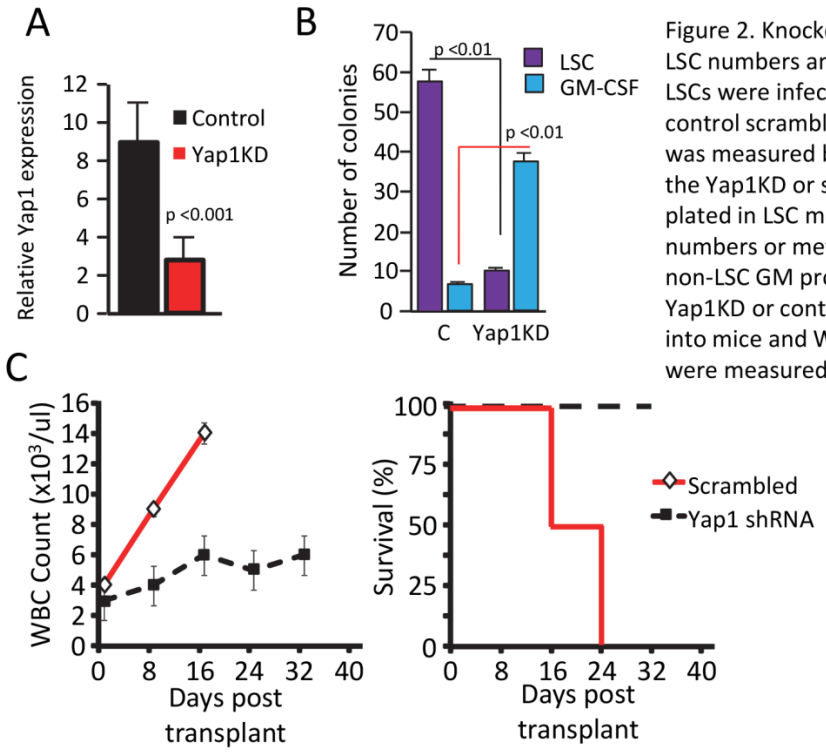


Figure 2. Knockdown of Yap1 expression decreases LSC numbers and blocks progression of disease. (A). LSCs were infected with a Yap1 shRNA virus or a control scramble virus. Relative Yap1 expression was measured by q-RT-PCR. (B) LSCs infected with the Yap1KD or scramble, C, shRNA viruses were plated in LSC methocel to assay LSC colony numbers or methocel containing GM-CSF to assay non-LSC GM progenitors. (C). LSCs infected with Yap1KD or control shRNA virus were transplanted into mice and WBC counts (left) and survival (right) were measured.

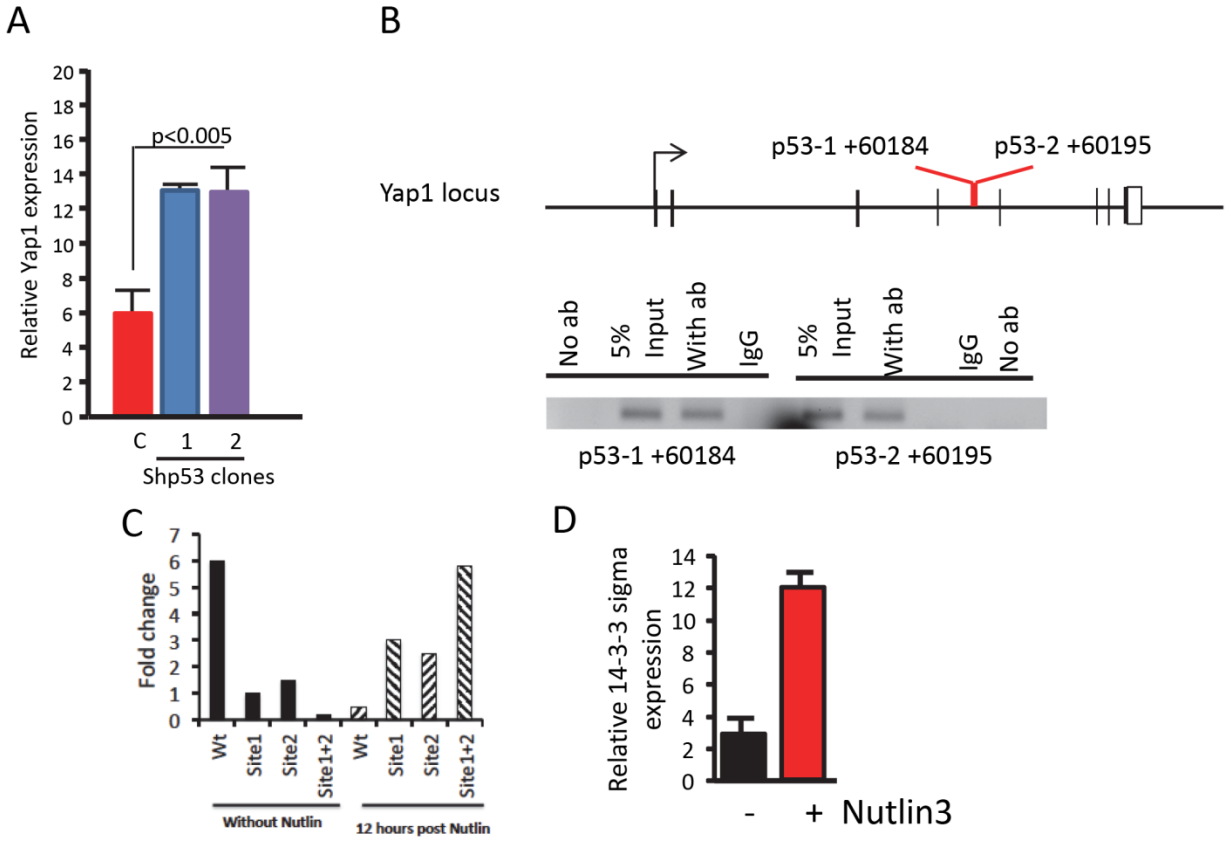


Figure 3. p53 regulates Yap1 expression. (A) CML LSCs were infected with scramble control , C, or a shRNA targeting p53 and Yap1 expression was measured using q-RT-PCR. (B) A schematic of the Yap1 locus with putative p53 binding sites indicated (top) . ChIP assays using an anti-p53 antibody and oligonucleotides corresponding to the two putative p53 binding sites. IgG indicates nonspecific IgG control antibody. (C). A fragment containing the two p53 binding sites was cloned upstream of a luciferase reporter gene. WT indicates wild type p53 binding sites and site 1, site 2 and site 1+2 indicate mutant versions of either site alone or both sites were cloned upstream of luciferase. Change in luciferase activity relative to a plasmid lacking the p53 sites was analyzed with and without Nutlin3 treatment to activate p53 activity. (D) Expression of 14-3-3 sigma expression in CML LSC ± Nutlin3 treatment.

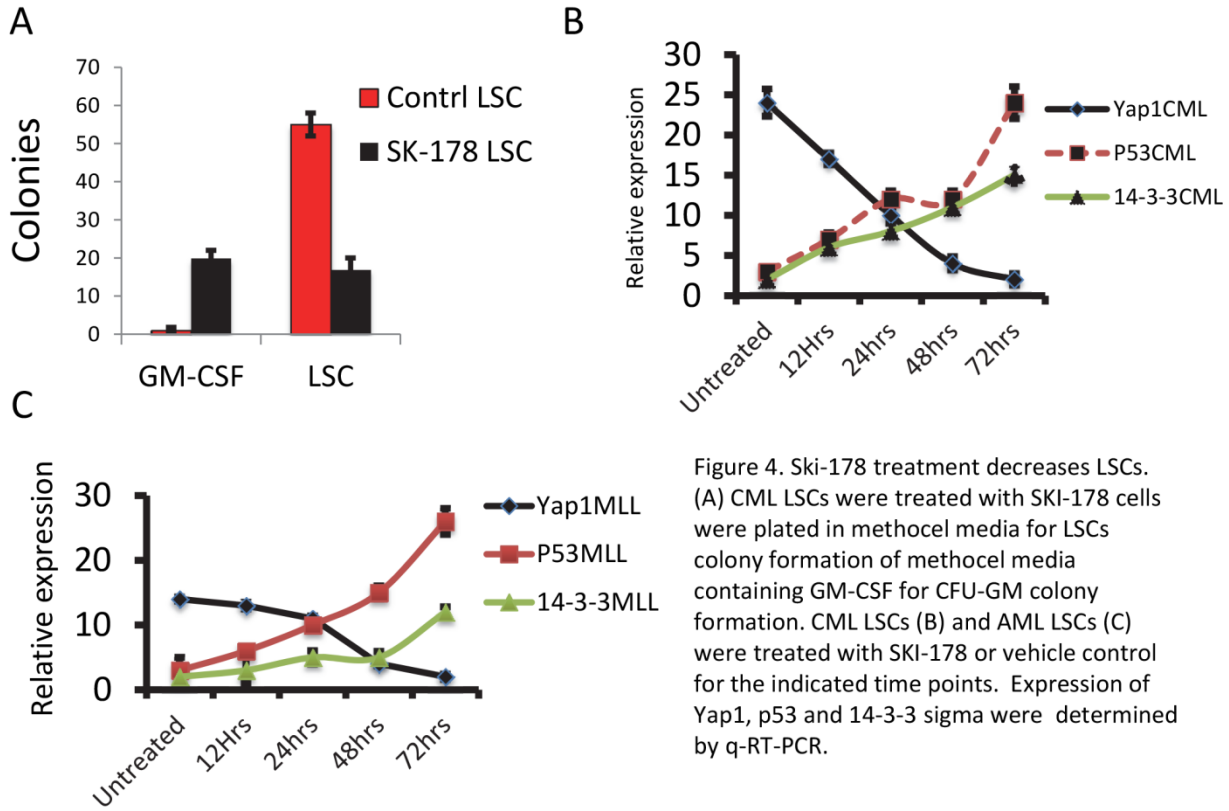


Figure 4. Ski-178 treatment decreases LSCs. (A) CML LSCs were treated with SKI-178 cells were plated in methocel media for LSCs colony formation of methocel media containing GM-CSF for CFU-GM colony formation. CML LSCs (B) and AML LSCs (C) were treated with SKI-178 or vehicle control for the indicated time points. Expression of Yap1, p53 and 14-3-3 sigma were determined by q-RT-PCR.

## Research Project 4: Project Title and Purpose

*Reprogramming HBV-specific CTL from Stem Cells for Cell-based Therapies* – Virus-specific T cells capable of controlling hepatitis B virus (HBV) and eliminating hepatocellular carcinoma (HCC) expressing HBV antigens are deleted or dysfunctional in patients with chronic HBV infection. Adoptive cell transfer (ACT) of highly reactive HBV-specific $CD8^+$ cytotoxic T lymphocytes (CTL) is a highly promising treatment for chronic HBV infection and HBV-related HCC. However, such ACT is often not feasible due to difficulties in obtaining these cells from patients. The studies in this project will define the unique properties of HBV-specific CTL derived from induced pluripotent stem cells (iPSC-CTL) and determine anti-HBV activity of iPSC-CTL.

### Anticipated Duration of Project

7/1/2013 – 12/31/2014

### Project Overview

The studies in this project will define the unique properties of HBV-specific CTL derived from iPSC (iPSC-CTL) and determine anti-HBV activity of iPSC-CTL. Our central hypothesis is that genetically modified iPSC with HBV-specific TCR, followed by differentiation driven by Notch

signaling will enable iPSC to pass positive and negative selections, resulting in development of highly reactive HBV-specific iPSC-CTL. We will test our central hypothesis through the following two Specific Aims:

1. *To define the unique properties of HBV-specific iPSC-CTL*
   (a) *Phenotypic analysis*. We will examine surface protein expression of T cell markers and activation proteins using fluorophore-conjugated Abs.
   (b) *Functional analysis.* We will stimulate iPSC-CTL with HLA-A2$^{+}$ stimulator cells pulsed with the cognate HBV peptide or the control peptide to determine the level of cytokine secretion, proliferation, expansion, survival, and cytotoxicity. After five days, we will isolate Ag-reactive CTL and re-stimulate to determine recall/memory responses.
   (c) *Sensitivity analysis*. We will co-culture iPSC-CTL with T2 cells loaded with various concentrations of HBV peptide. We will examine the mean percent of maximum IFN-γ response obtained from intracellular cytokine staining.

2. *To determine the anti-HBV activity of HBV-specific iPSC-CTL*

We will use Rag2$^{-/-}$ γc$^{-/-}$ mice to evaluate the cytotoxicity of iPSC-CTL *in vivo*. We will inject *s.c* HBV core expressing HepG2 cells into the flank. We will allow tumors to form for 15 d. We will then introduce iPSC-CTL into the tumor site to determine their anti-HBV activity. We will also investigate T cell persistence. We will track the transferred T cells from the spleen, lymph nodes, and tumor tissues at different times by analyzing the TCRVβ12$^{+}$ CD8$^{+}$ population and determining CTL activation and cytokine production, function and memory.

**Principal Investigator**

Jianxun Song, PhD
Assistant Professor
Pennsylvania State University College of Medicine
Department of Microbiology and Immunology
500 University Dr.
Hershey, PA 17033

**Other Participating Researchers**

Fengyang Lei, MBBS, Kristin Fino, PhD – employed by Pennsylvania State University

**Expected Research Outcomes and Benefits**

We expect that iPSC-CTL generated by our approach will be naive HBV-specific CTL, which will respond to HBV stimulation and secrete IFN-γ as well as express HBV-specific cytotoxicity similar to the original HBV-specific CTL clone. In addition, ACT of HBV-specific iPSC-CTL will significantly inhibit HBV$^{+}$ tumor growth in the murine model.

The research will provide new insight and strategies for generating highly reactive HBV-specific T cells from pluripotent stem cells and in so doing drive forward use of therapeutic T cells for

the treatment of HBV infections and HBV-related HCC.

**Summary of Research Completed**

*Aim 1: To define the unique properties of HBV-specific iPSC-CTL*

(a) *Phenotypic analysis*.
We retrovirally transduced human iPSC (iPS-DF6-9-9T.B, vector-free iPSC, the WISC Bank) with the human HBV ($HBs_{370-379}$-specific - s370) TCR gene. The TCR gene-transduced iPSC were then co-cultured with OP9-DL1/DL4/HLA-A2 cells expressing Notch ligands (both DL1 and DL4) and HLA-A2 molecules in the presence of Flt3L, IL-7 and IL-15. A 2-wk co-culture generated HBV-specific $CD4^-CD8^-$ double negative (DN) pre-T cells ($CD3^+TCRV\beta7^+$; $CD25^+CD44^-$), and a 4-week co-culture gave rise to HBV-specific $CD3^+TCR^+$ $CD4^-CD8^+$ single positive (SP) T cells (**Fig. 1-3**). In addition, we have observed an approximately 38,000-fold increase of cell numbers on day 28 and 87% of these cells are HBV-specific SP CTL. *These data show that HBV-specific iPSC-CTL are naive single-type T cells and can be used to generate highly reactive HBV-specific CTL.*

(b) *Functional analysis.*
On day 28, HBV-specific $CD8^+$ T cells ($CD3^+TCR\beta7^+CD8^+$) were sorted and their functional activities were assessed. We stimulated iPSC-CTL with HLA-$A2^+$ stimulator cells pulsed with the cognate HBV peptide or the control peptide to determine the level of cytokine secretion, proliferation, expansion, survival, and cytotoxicity. After five days, we isolated Ag-reactive CTL and re-stimulated to determine recall/memory responses.

We observed: (1) iPSC-CTL secreted large amounts of IFN-γ; and (2) iPSC-CTL displayed Ag-specific cytotoxic activity (**Fig. 2**). *These data demonstrate that HBV-specific iPSC-CTL are functional and have a potential to be used in cell-based therapies of chronic HBV infection and HBV-associated liver cancers.*

(c) *Sensitivity analysis*.
We co-cultured iPSC-CTL with T2 cells loaded with various concentrations of HBV peptide. We examined the mean percent of maximum IFN-γ response obtained from intracellular cytokine staining. We found that the sensitivity of the HBV-specific iPSC-CTL was similar to the original HBV-specific CD8 T cell clone (**Fig. 3**)

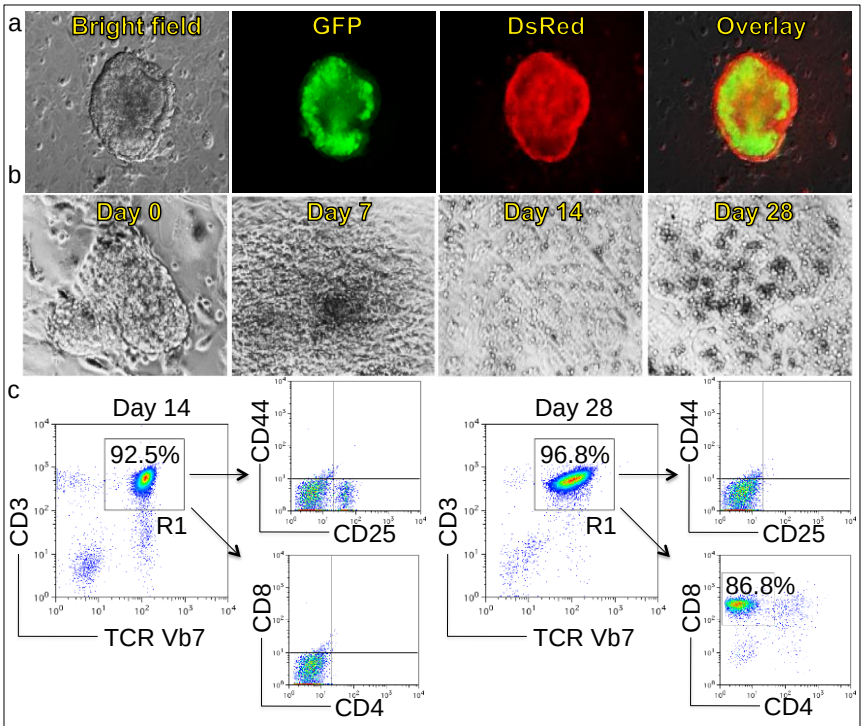


**Fig. 1 Generation of HBV-specific PSC-CTL *in vitro.*** Method: s370 HBV TCR gene (Va12, Vb7)-transduced iPSC (DsRed$^+$) were sorted and co-cultured on OP9-DL1/DL4/HLA-A2 cells in the presence of Flt3L, rIL-7 and rIL-15. **(a)** Morphology of TCR gene transduction of iPSC. **(b)** Morphology of T-cell differentiation of iPSC on OP9-DL1/DL4/HLA-A2 cells on days 0, 7, 14, and 28. **(c)** On days 14 and 28, expression of CD3 and TCRVb7 on iPSC-CTL was analyzed by flow cytometry. CD3$^+$ TCR Vb7$^+$ cells were gated (R1), and analyzed for expression of CD25 and CD44 or CD4 and CD8.

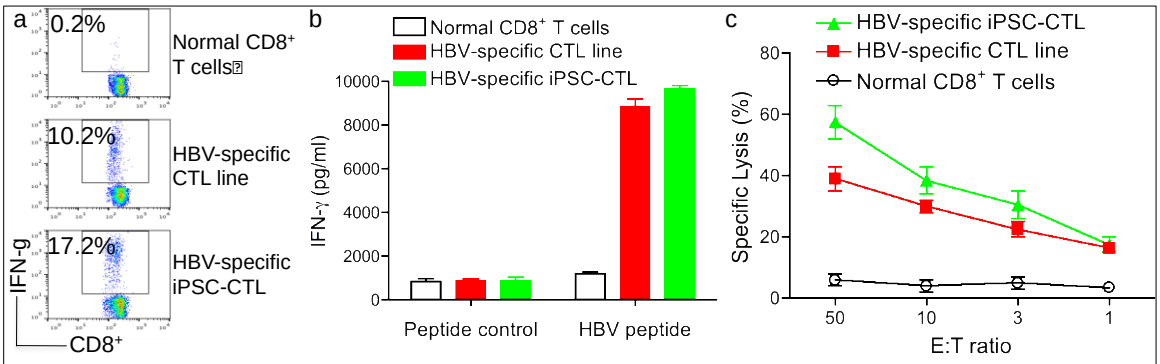


**Fig. 2 Reactivity measurement of HBV-specific PSC-CTL.** Method: s370 HBV-specific iPSC-CTL, s370 HBV-specific CTL line, and normal human CD8$^+$ T cells from healthy donors (HLA-A2$^+$) were incubated with T2 cells (a-b) or $^{51}$Cr-labeled HepG2 target cells (c) pulsed with s370 HBV-specific peptide or a control peptide. **(a)** IFN-g by intracellular staining after 5 hr, gated on CD8$^+$ cells. HBV peptide pulsed. **(b)** IFN-g by ELISA after 20 hr. **(c)** Lysis was assessed by radioactivity of supernatant following coculture for 4 hr. Graph shows the specific lytic activity of cells at different effector to target cell ratio.

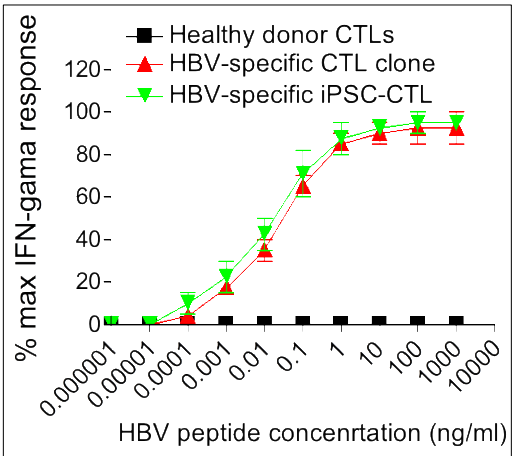


**Fig. 3 Sensitivity of activation of HBV-specific iPSC-CTL.** Method: HBV-specific iPSC-CTL, original HBV-specific CTL clone, and healthy donor were co-cultured with HBV specific peptide (FLPSDFFPSV)-loaded T2 cells for 5 hr. Results are displayed as mean percent of maximum IFN-g response obtained from intracellular cytokine staining.

## Research Project 5: Project Title and Purpose

*Investigating the Mechanisms of Esophageal Squamous Cell Carcinoma Invasion* – Esophageal squamous cell carcinoma (ESCC) is the most prevalent form of esophageal cancer throughout the world and carries a dire prognosis, primarily due to presentation at an advanced stage and the invasiveness of the disease. The Epidermal growth factor receptor (EGFR) gene is commonly overexpressed in almost 90% of ESCC tumors. Another gene, p120ctn, is frequently down-regulated in approximately 60% of ESCC tumors. Esophageal cells that have been altered to have decreased p120ctn expression and overexpression of EGFR invade the extracellular matrix in a 3D-culture system. Our project proposes to define the mechanisms by which p120ctn and EGFR cooperate to synergistically influence esophageal squamous cell carcinoma invasion.

### Duration of Project

1/1/2013 – 12/31/2013

### Project Overview

When the Epidermal growth factor receptor (EGFR) gene is overexpressed and the p120ctn gene expression is decreased, it results in transformation of esophageal keratinocytes and cellular invasion in our *in vitro* 3D culture system. Therefore, based on our observations, the experimental focus of this project is on the intersection of p120ctn and EGFR and the mechanisms behind how these two cooperate to cause an invasive phenotype. We hypothesize

that when p120-catenin is down-regulated and EGFR is overexpressed specific gene networks play an integral role in modulating the invasive phenotype of esophageal squamous cell carcinoma.

Specific Aims:
Aim 1: Identify genes that induce/modulate esophageal squamous cell carcinoma invasion. We will analyze genes known to be regulated by both p120 and EGFR (Rho GTPases, Stat3, and the Src pathway). This analysis will be performed by examining their expression and activation by western analysis and GTP pull-down assays. Additionally, RNA will be harvested from our cell lines that overexpress EGFR and have decreased p12ctn expression. Gene expression microarray analysis will be performed to generate lists of differentially expressed genes. Genes from these lists will be validated and subsequent functional analyses will be performed to test the involvement of these genes in invasion in our culture system.

Aim 2: Determine gene expression in patient samples. We will verify pathway alterations seen in our culture system with findings in human ESCC tissue. Publically available microarray data sets on human ESCC will be compared to the microarray data generated in Aim 1. As well, human ESCC patient samples will be stained by immunohistochemistry for p120ctn, EGFR, and genes found to be involved in invasion subsequent to p120ctn knockdown and EGFR overexpression in Aim 1. These experiments in addition to those in Aim 2A will strengthen the relevance of these genes in ESCC and suggest they may be potential therapeutic targets for the treatment of ESCC.

**Principal Investigator**

Douglas B. Stairs, PhD
Assistant Professor
Pennsylvania State University
500 University Drive
Hershey, PA 17033

**Other Participating Researchers**

Heather Lehman, PhD; Anna Salzberg, MS – employed by Pennsylvania State University

**Expected Research Outcomes and Benefits**

By performing the research outlined here, we will discover novel signaling pathways involved in esophageal tumor cell invasion. The molecular pathways downstream of p120ctn are largely unknown in any cancer type. Investigating p120ctn together with EGFR in relation to ESCC (as well as all cancers) is novel. The intersection of two genetic events and how they cooperate synergistically to lead to the invasive phenotype has not been studied in esophageal cancer previously. We will employ a 3D culture system which uniquely recreates the normal differentiation program of the esophagus and allows for *in vitro* analysis of cellular invasion. Our culture results will be analyzed against human ESCC samples to verify that what we identify *in vitro* is seen in the human ESCC. Taken together, this project uses highly innovative and novel

approaches to mechanistically study the invasive phenotype of ESCC.

**Summary of Research Completed**

Aim 1:
Further work was performed with the microarray expression data generated from our 3D culture system. Subcategory analysis of the Cancer Gene Ontology Category demonstrates the relevance of the gene changes seen in cells with p120ctn down-regulation and EGFR overexpression (EPC1-PE cells). All of the top 10 subcategories are related to metastasis in general, to gastrointestinal cancers or to squamous cancers (Table 1).

Analysis of our gene expression list from the Metastasis subcategory identified an EMT-regulating transcription factor, Twist 2, as being increased in EPC1-PE cells. Based upon microarray expression, Twist2 increased 11.4-fold. Quantitative PCR of Twist2 revealed a 3-fold increase in EPC1-PE cells when compared to control EPC1 cells. These data suggest that EMT processes may be involved in EPC1-PE cell invasion.

Several Keratins (Krt) have been implicated in cancer invasion and analyses of our microarray data have identified four keratins that decreased and one that increased in EPC1-PE cells compared to control EPC1 cells. Krts 1,4,10 and 15 are down-regulated 13-fold, 11-fold, 5-fold and 4-fold respectively while Krt 8 is up-regulated 4-fold in EPC1-PE cells.

Aim2:
Aim 2A was to compare gene expression microarray lists of our 3D culture with ESCC patient microarray data. At a first approximation, we compared the global lists of each 3D culture to those of ESCC classified as no change in p120ctn or EGFR, p120ctn down-regulation by itself, EGFR up-regulation by itself or both p120ctn down-regulation and EGFR up-regulation. Interestingly, the magnitude of gene expression similarities is similar between all groups (Table 2). Therefore, there is no "enrichment" of gene expression in ESCC and 3D culture samples with similar gene expression patterns of p120ctn and EGFR. This does not preclude the possibility of genes found on both lists having an important role in the pathogenesis of cancer involving p120ctn down-regulation and EGFR overexpression.

Aim 2B was to validate potential genes of interest identified in Aim 1 as being altered in their expression in ESCC. We have microarray and qPCR data suggesting EMT to be involved in the invasion of EPC1-PE cells (see above). We further tested this hypothesis by performing Western blot analysis for E-cadherin and Twist2. E-cadherin expression decreased with p120ctn deletion (control versus EPC1-P cells) but was further suppressed in EPC1-PE cells suggesting that both p120ctn and EGFR are contributing to E-cadherin loss (Figure 1A). It is firmly established that p120ctn loss destabilizes E-cadherin and therefore this is likely the explanation for its down-regulation in EPC1-P cells. Twist2 protein expression is upregulated in EGFR overexpressing cells (Figure 1B). The combination of p120ctn down-regulation and EGFR overexpression in EPC1-PE cells may explain the approximately 20-fold decrease in E-cadherin expression compared to control cells. Work will be continued to determine the expression of Twist2 in ESCC samples.

As mentioned above, several keratins have altered expression in our 3D culture system based on our microarray results (see above) and have also been reported previously in ESCC. We tested whether the keratin changes in our culture system were similar to that seen in ESCC. We assembled a panel of 24 de-identified ESCC samples and 10 independent normal esophagi samples for use in these experiments in collaboration with an anatomic pathologist. H&E staining was performed and reviewed by our pathologist for accuracy of diagnosis. Immunohistochemistry (IHC) on these human samples as well as on 5 independent replicates of 3D cultures was performed for p120ctn, EGFR, Krt1, Krt4, Krt8, Krt10 and Krt15 (Figure 2). Staining for p120ctn and EGFR validated the genetic manipulations performed in our 3D culture and demonstrated that approximately 60% of our cultures had decreased p120ctn expression and EGFR overexpression as would be expected. Krt1does not change in expression in ESCC or in our culture system. Krt4, Krt10 and Krt 15 all decrease in both ESCC samples and in EPC1-PE cells when compared to their respective control samples. Krt 8 has a slight increase in staining in ESCC but no increase was observed in EPC1-PE cells. In summary, four of five keratins change profiles identically in ESCC and in 3D cultures of EPC1-PE cells.

| Category | Function Subcategory | p-value |
|---|---|---|
| **Cancer** | **Metastasis** | **8.11E-11** |
| **Cancer** | **Metastatic colorectal cancer** | **1.08E-09** |
| **Cancer** | **Gastrointestinal tract cancer and tumors** | **1.42E-06** |
| **Cancer** | **Endometrial cancer** | **1.65E-06** |
| **Cancer** | **Gastrointestinal tumor** | **2.16E-06** |
| **Cancer** | **Gastrointestinal tract cancer** | **2.56E-06** |
| **Cancer** | **Head and neck tumor** | **5.68E-06** |
| **Cancer** | **Intestinal cancer** | **6.15E-06** |
| **Cancer** | **Colorectal cancer** | **7.44E-06** |
| **Cancer** | **Head and neck cancer** | **1.21E-05** |

**Table 1** Top gene ontology classifications when p120ctn is down-regulated and EGFR is overexpressed. Cancer is the top category with genes involved in metastasis indicated as the most significant functional subcategory.

| | | 3D Cultures | | | |
|---|---|---|---|---|---|
| | | **Control** | **p120ctn ↓** | **EGFR ↑** | **p120ctn↓ EGFR ↑** |
| **GSE20347** | **Control** | 25.1 | 25.6 | 25.2 | 23.8 |
| | **p120ctn ↓** | 34.5 | 34.7 | | |
| | **EGFR ↑** | 29.4 | | 29.3 | |
| | **p120ctn ↓ EGFR ↑** | 36.4 | | | 35.1 |
| **GSE23400** | **Control** | 28.2 | 28.4 | 27.8 | 27.1 |
| | **p120ctn ↓** | 20 | 20.3 | | |
| | **EGFR ↑** | 30.5 | | 30 | |
| | **p120ctn ↓ EGFR ↑** | 20.6 | | | 19.3 |

**Table 2** Comparisons of p120ctn down-regulation and EGFR overexpression in 3D cultures and GEO human data sets. In these data sets p120ctn and EGFR expression independently segregate.

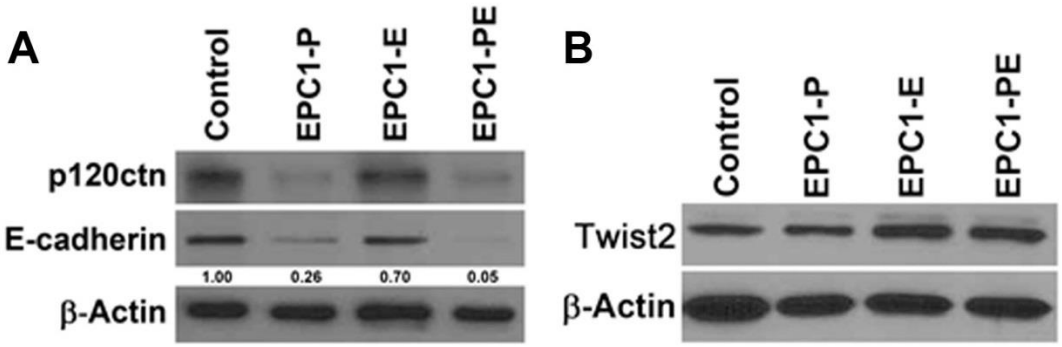


**Figure 1 A:** E-cadherin and Twist2 expression in EPC1-hTERT cells. Western blot analysis demonstrates a decrease in E-cadherin protein levels when p120ctn is down-regulated in EPC1-P and a further decrease in E-cadherin expression in EPC1-PE cells. β-actin is used as a loading control. Band intensity was quantified by densitometry and normalized to EPC1-hTERT β-actin. Values are expressed as relative to the EPC1-hTERT control. **B:** Western blot analysis demonstrates a slight increase in Twist2 protein expression in EPC1-PE cells compared to EPC1-hTERT control cells. β-actin was used as a loading control.

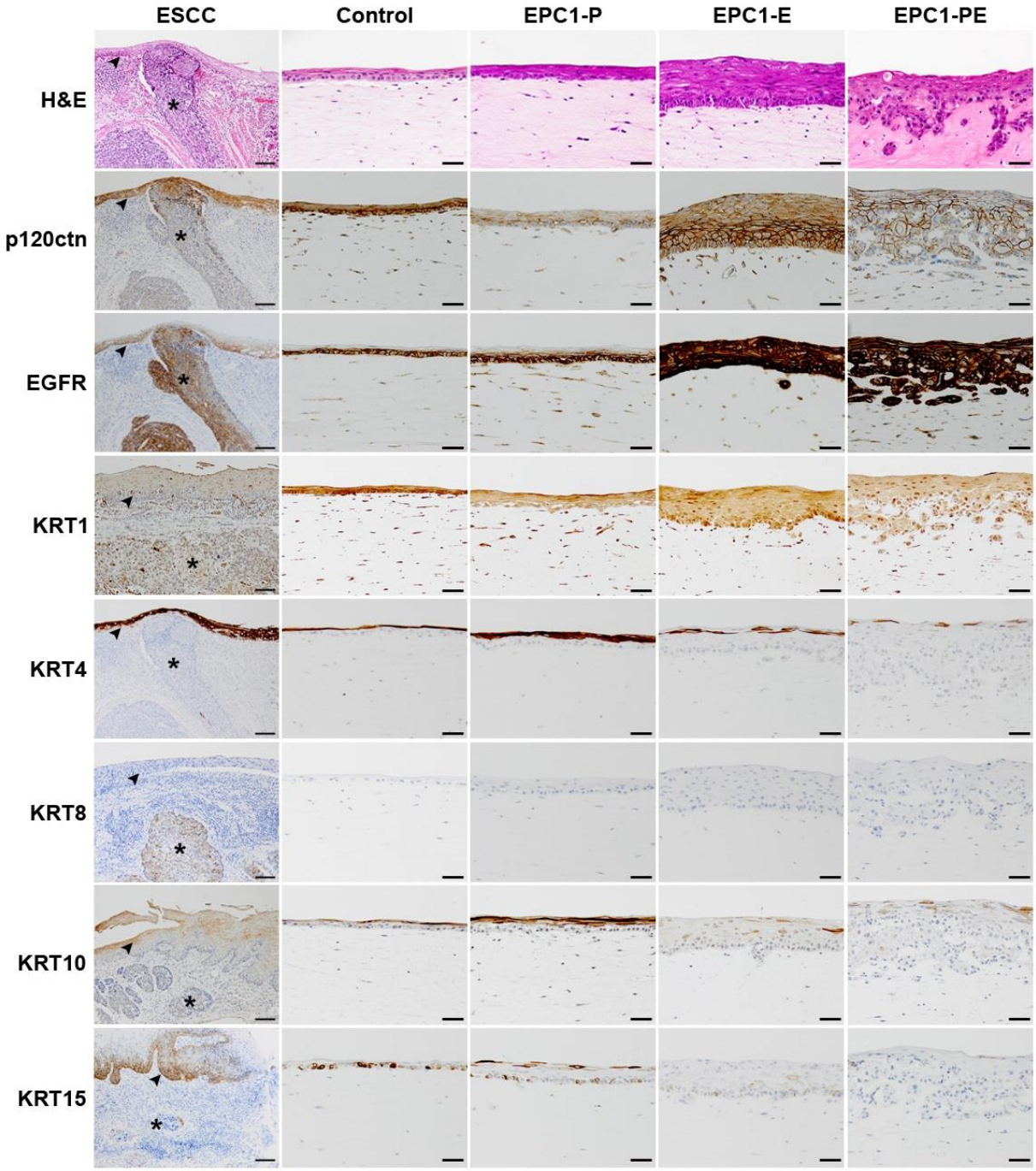


**Figure 2** IHC analyses of human ESCC and 3D cultures. p120ctn expression is decreased and EGFR is increased in human ESCC tissue compared to normal-appearing adjacent (control) esophageal epithelium. IHC demonstrates a knockdown in p120ctn EPC1-P and EPC1-PE 3D cultures and overexpression of EGFR in EPC1-E and EPC1-PE cultures. IHC staining of human ESCC demonstrates that KRT1 expression does not change in ESCC. Expression of KRT4 is lost while KRT10 and KRT15 are decreased in ESCC compared to control epithelium. Weak and focal KRT8 expression is gained in ESCC. Keratin expression in EPC1-PE 3D cultures is nearly identical to human ESCC. Arrowhead=control epithelium; asterisk=ESCC. Scale bars: 50 μm.

## Research Project 6: Project Title and Purpose

*Immunological and Anti-tumor Mechanisms of LipC6 Treatment in a Murine Model of HCC –* We have established a novel murine model which uniquely approximates hepatocellular carcinoma (HCC) tumor progression, tumor morphology, microenvironment with liver fibrosis. Using this model, we will initially determine the role of LipC6 in modulating a variety of subset T cells and preventing tumor antigen-specific CD8 T-cell tolerance in vivo; then we will determine the role of LipC6 alone and in combination with adoptively transferred TCR-I T cells in HCC treatment. The results will be used to further apply for an R01 grant sponsored by NIH. The knowledge gained will lay the foundation for translational approaches in human HCC that combine LipC6 with new or existing immunotherapies.

### Duration of Project

5/1/2013 – 6/30/2014

### Project Overview

Hepatocellular carcinoma (HCC) is the third leading cause of cancer mortality worldwide, and continues to increase in the US as the result of Hepatitis C infection. The high rate of mortality, frequent incidence of recurrence, and limited benefit of current therapies for this disease reveal the urgent need for new therapeutic approaches.

C6 ceramide nano liposomes (LipC6) have demonstrated antitumor activity in a number of tumor types. Using human HCC cell xenografts into nude mice and our orthotopic model, we have demonstrated that LipC6 promotes reduction in tumor size. In addition we have shown that treatment with LipC6 reverses immunotolerance and works in combination with immunotherapy to induce regression of tumors.

The overall objective of this project is to elucidate the cellular mechanisms by which LipC6 prevents HCC-induced immunotolerance. We will additionally evaluate the synergistic effect of combined LipC6 and tumor specific immunotherapy for HCC treatment. We will approach our objectives through the following specific aims:

Aim 1: Define the cellular and molecular mechanisms through which LipC6 prevents tumor antigen-specific CD8 T-cell tolerance in vivo. We will compare the frequency, phenotype and function of CD8 T cells, regulatory T cells, myeloid and dendritic cells in tumor-bearing mice treated with LipC6 or control ghost and define the molecular pathways involved in this process.

Aim 2: Determine the efficacy of LipC6 treatment alone and in combination with immunotherapy on HCC progression. We will evaluate the independent and synergistic effects of LipC6 and adoptive CD8 T-cell transfer to control HCC growth.

**Principal Investigator**

Todd Fox, Ph.D
Assistant Professor of Pharmacology
The Pennsylvania State University
College of Medicine
500 University Drive
Hershey PA 17033

**Other Participating Researchers**

Guangfu Li, PhD; Mark Kester, PhD; Todd Schell, PhD; Jeremy Haley – employed by The Pennsylvania State University College of Medicine; Kevin Staveley-O'Carroll MD, PhD, Guangfu Li – employed by the Medical University of South Carolina; Mark Kester, PhD, employed by the University of Virginia.

**Expected Research Outcomes and Benefits**

LipC6 treatment is expected to reduce the frequency of regulatory T cells (Tregs) and myeloid-derived suppressive cells (MDSCs) in tumor-bearing mice and suppress secretion of TGF-β and IL-10 in immune cells, potentially releasing their suppressive effects. LipC6 treatment will likely activate CD8 T cells to produce IFN-γ, TNF-α, perforin, granzyme B in response to tumor-specific antigens, killing tumor cells. We may find that LipC6 alters the distribution of DC subtypes in the liver and spleen of tumor-bearing mice, promoting an increase of matured DC subtypes. Low expression of CD80, MHC class II and CD40 would be consistent with an immature phenotype and tolerogenic properties. Such results would lead us to further examine the functional properties of the affected subsets.

In addition, we expect that LipC6 treatment will suppress Akt, Stat3 and PI3K pathways which are implicated in tumor growth and immunotolerance, but we may find that LipC6 has differential effects compared to sunitinib which would lead us to further examine the pathways that are interrupted or activated.

In vivo experiments to assess the therapeutic efficacy of LipC6 will be conducted, and LipC6 treatment is expected to suppress tumor growth in vivo; and the combination of LipC6 and TCR-I T cells will promote additional tumor growth suppression. Such results would lead us to develop a novel and effective combined therapeutic strategies for HCC through incorporating with immunotherapy.

The success of this project will potentially extend the life of patients and reduce the economic and social burden of this lethal disease.

**Summary of Research Completed**

We have made significant progress during the grant period (7/1/13- 6/30/14) despite a significant change of leadership. Dr. Todd Fox is now PI on the grant working closely with Dr. Todd Schell

of Penn State. Dr. Staveley-O'Carroll and Dr. Guangfu Li transferred to the Medical University of South Carolina while Dr. Mark Kester is now the Director of the nanoSTAR Institute of the University of Virginia. Drs. Fox and Schell are still working with Drs. Staveley-O'Carroll, Li and Kester investigating the role of Lip C6 in a fibrotic, cirrhotic model of primary liver cancer.

*Aim 1*

Specifically, significant progress has been made in documenting that Ceramide (Lip C6) breaks tumor-induced immunotolerance and serves as an immunomodulatory agent. LipC6 has shown additional immunomodulatory benefits. Pharmacological inhibition of ceramide production by the fungal toxin B1 impairs TCR-induced interleukin (IL)-2 production and programmed cell death, but the addition of either exogenous ceramide or bacterial sphingomyelinase to enhance endogenous ceramide can reconstitute both responses. Moreover, specific inactivation of neutral sphingomyelinase by antisense RNA inhibited IL-2 production and mitogen-activated protein-kinase activation after TCR triggering. These results suggest that ceramide production by activation of neutral sphingomyelinase is an essential component of the TCR signaling machinery. Using our high-fidelity murine model, we demonstrated that LipC6 alone significantly slows down tumor growth, but is not sufficient to destroy tumors. Interestingly, LipC6 breaks tolerance and restores CD8 T-cell activity, such that, in combination with immunotherapy, this treatment eradicates established tumors (Fig 1). *These results suggest that LipC6 is a clinically-available agent and effective targeted/immunomodulatory mediator which can synergistically work with immunotherapy for HCC treatment.*

*Aim 2*

We next investigated the mechanism(s) by which LipC6 modulates this anti-tumor response and serves as an effective immunomodulatory agent in HCC. We have previously demonstrated that LipC6 exerts growth-arresting and pro-apoptotic function in HCC cells. We found that LipC6 treatment led to the accumulation of SK-Hep-1 cells in the G2 phase of the cell cycle, and induced apoptotic cell death associated with the decreased phosphorylation of AKT. Using a xenograft model in which SK-Hep-1 cells were engrafted subcutaneously into immunodeficient nude mice, we demonstrated that systemic administration of LipC6 by IV injection reduces tumor vascularization, induces tumor cell apoptosis, and decreases AKT phosphorylation in tumors; ultimately, blocking tumor growth. Using our recently-established, innovative and clinically-relevant murine model, we demonstrated that LipC6 alone noticeably slows down tumor growth but is not sufficient to shrink tumors (Figure 1). Interestingly, treatment with LipC6 prevents the tumor-induced reduction of adoptively transferred TCR-I T cells, breaks tumor-induced immunotolerance, and restores effector CD8 T-cell activity in response to immunization with tumor-specific antigens (Figure 2). Furthermore, the combination of LipC6 and immunotherapy eradicates established tumors (Figure 1). *These results suggest that LipC6 capably modulates anti-tumor immune response and serves as an effective immunomodulatory agent in HCC.*

These provocative findings drove us to investigate the underlying cellular and molecular mechanisms. At the cellular level, LipC6 may directly work on the effector CD8 T cell or indirectly modulate other immune cell subsets to activate anti-tumor immunity. Our initial investigation demonstrated that LipC6 treatment did not significantly reduce the frequency of regulatory T cells (Treg) (Figure 3) Tregs are recognized as one of several critical immune-

suppressive cells, and they are associated with tumor-induced immune tolerance. Further, we demonstrated that LipC6 treatment results in a phenotype change in macrophages (MΦ). Macrophages are prominent components of solid tumors and exhibit distinct phenotypes in different microenvironments. In addition, macrophages are known to contribute to tumor evasion from the immune system. Flow cytometry showed that LipC6 treatment reduced the $CD206^{+}F4/80^{+}M\Phi$ population and increased the $CD86^{+}F4/80^{+}M\Phi$ population in peritoneal macrophages from tumor-bearing mice (Figure 4). LipC6 treatment was found to cause up-regulation of CD86 (M1 macrophage marker), and reduction of CD206 (M2 macrophage marker) in tumor tissue (Figure 5a). IHC further confirmed these results in the liver tissues from the indicated mice (Figure 5b). *These results suggest that LipC6 mediates the macrophage polarization from M2 to M1 and may contribute to the activation of an anti-tumor immune response.*

We next investigated the molecular mechanism by which Lip C6 mediates macrophage polarization. As one of the first cytokines to be discovered, macrophage inhibitory factor (MIF) has been demonstrated to be overexpressed in many solid tumors, inhibits the random migration of macrophages *in vitro,* and facilitates tumor proliferation and evasion of apoptosis. In addition, MIF is known to be involved in angiogenesis and metastasis. In HCC, MIF was demonstrated to be highly expressed, plays an important role in the tumor progression, and could be used as a marker for HCC tumor detection. Using our recently-established, innovative and clinically-relevant murine model, we demonstrated that tumor growth causes the up-regulation of MIF in tumor tissue, and the treatment with LipC6 prominently reduces MIF to the level in liver tissue from normal syngeneic mice (Fig.6). Also, treatment of tumor-bearing mice with LipC6 noticeably reduces the expression of MIF in macrophages (Fig 7). In addition, we found that LipC6 treatment prevents tumor-induced immunotolerance and works in combination with tumor antigen-specific T cell to eradicate the established tumors (Fig.1). *These results suggest that LipC6-mediated reduction of MIF in tumors, macrophages, and other immune cells may contribute to the activation of an anti-tumor immune response.*

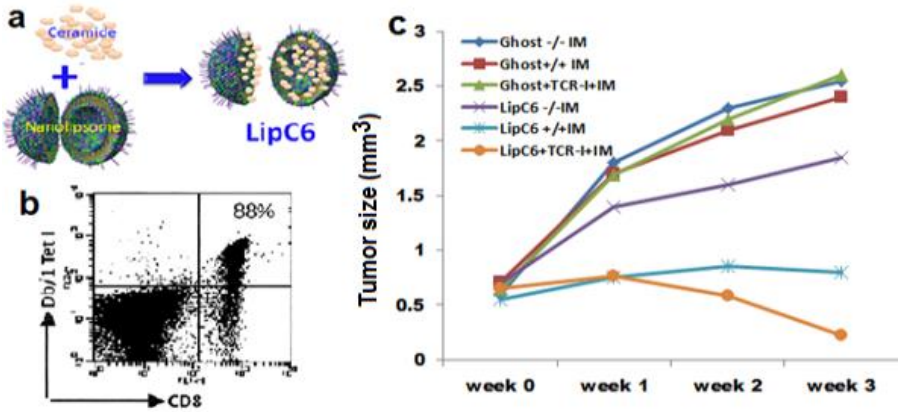


Figure 1. The anti-tumor/immunomodulatory effect of LipC6 in HCC. a. Nanotechnology is used to make nanoliposome-loaded ceramide (LipC6). b. The frequency of tet-I$^{+}$CD8$^{+}$ T cells (TCR-I) in CD8 T-cell receptor for T antigen epitope-I transgenic mouse. Lymphocytes from lymph nodes and spleen in 416 mice are stained with fluorochrome-conjugated CD8 and tetramer-I and then used to conduct the flow cytometry assay for determining the frequency of TCR-I in CD8 T cell. c. Combination of LipC6 treatment and TCR-I T-cell following by immunization with Tag-transformed B6/WT-19 cells shrink the established tumors in our clinically-relevant murine model. Tumor-bearing mice with the comparable tumor volume are received IV injection of LipC6 every other day for two weeks at a dose of 35 mg/kg, following by IV adoptive transfer of $1\times10^{6}$ TCR-I T cells and subsequent IP immunization with$3\times10^{7}$ B6/WT-19 cells. Weekly Magnetic Resonance Imaging (MRI) is conducted to monitor tumor growth. The represent results in one experiment are shown.

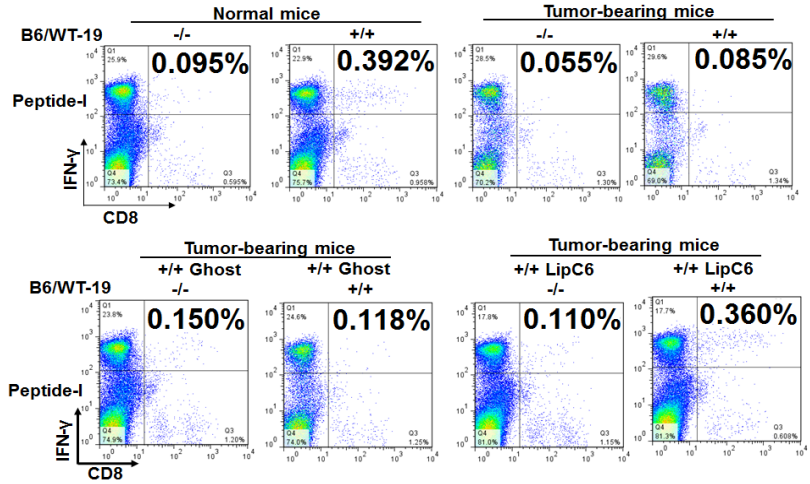


Figure 2. LipC6 treatment restores the activity of tumor-specific CD8$^{+}$ T-cell. The Tumor-bearing mice were treated with LipC6 every other day for consecutive two weeks at a dose of 35mg/Kg of body weight, then received adoptive transfer of TCR-I T cells (CD8 T cell for tumor antigen-specific epitope I) and immunization with B6/WT-19 cells (tumor antigen transformed cells). 5 days late, the splenocytes were isolated to measure the IFN-γ production in CD8 T cell in response to stimulation with tumor antigen-specific epitope *in vitro*. The normal mice and tumor-bearing mice received vehicle treatment (Ghost) are used for control.

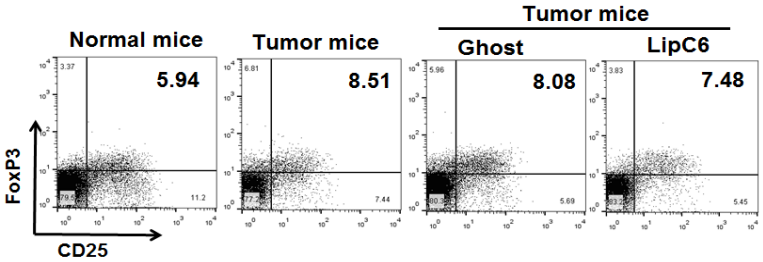


Figure 3. LipC6 treatment doesn't alter the magnitude of Treg in tumor-bearing mice. Isolated splenic lymphocytes from tumor-bearing mice treated with LipC6 or vehicle were used to perform FACS. The representative dot plot shows the expression of CD25 and FoxP3 on splenocytes gated on CD4 T cell.

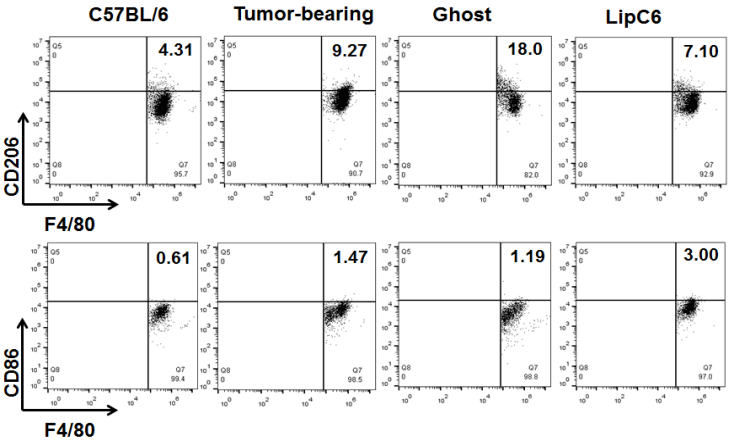


Figure 4. LipC6 treatment modulates the magnitude of M1 and M2 macrophage. Isolated peritoneal macrophages from tumor-bearing mice treated with LipC6 or vehicle were used to perform FACS. The representative dot plot shows the expression of CD206 and F4/80, and CD86 and F4/80 on macrophages gated on F4/80 macrophages.

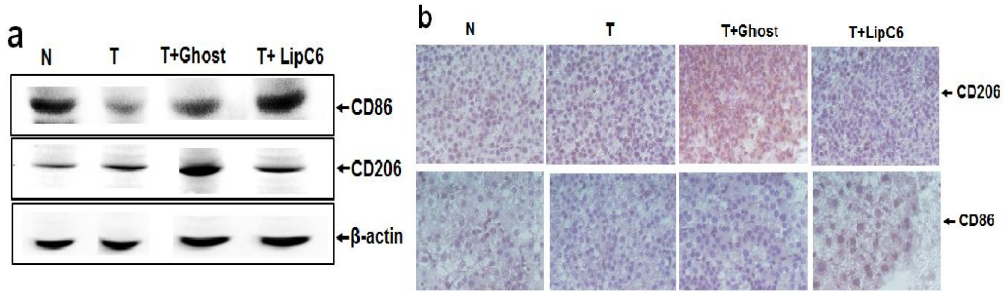


Figure 5. LipC6 treatment modulates the expression of CD206 and CD86 in tumor-bearing mice. Tumor-bearing mice are treated with LipC6 every other day by IV injection for consecutive two weeks. The indicated tissues were harvested to perform western blot (a) and IHC (b). The results reveal that LipC6 treatment results in the decrease of CD206 and increase of CD86 protein expression in the tumor-bearing mice.

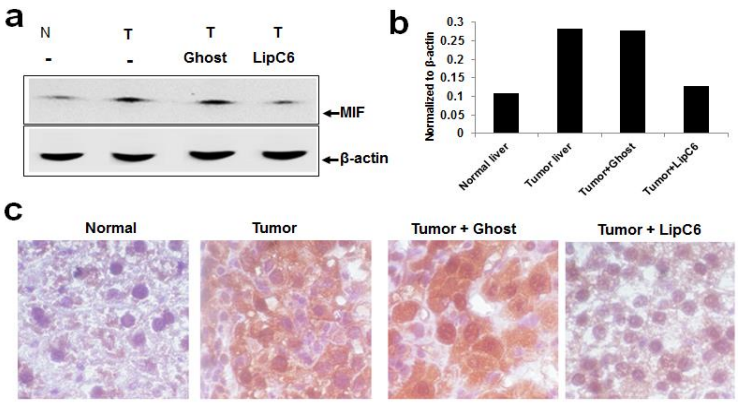


Figure 6. In vivo treatment of tumor-bearing mice with LipC6 suppresses tumor-mediated MIF up-regulation. Tumor-bearing mice are treated with LipC6 every other day by IV injection for consecutive two weeks. The indicated tissues were harvested. a. Western blot showed that LipC6 treatment down-regulate MIF protein expression in the tumor-bearing mice. b. The relative level of MIF protein expression is normalized to β-actin. c. IHC showed that LipC6 treatment down-regulate MIF protein expression in the tumor-bearing mice.

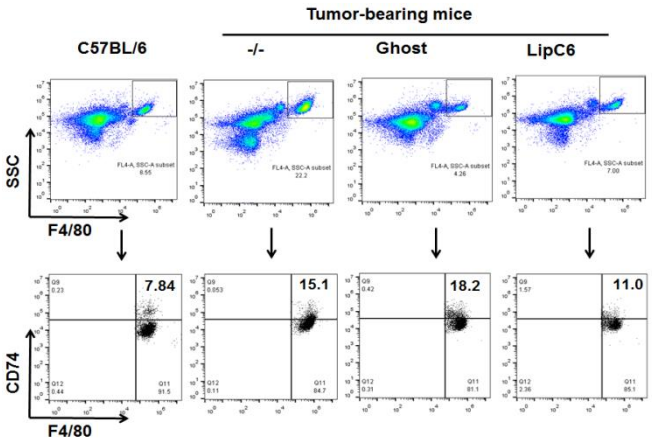


Figure 7. In vivo treatment of tumor-bearing mice with LipC6 results in the reduction of frequency of $MIF^{+}M\Phi$. Tumor-bearing mice are treated with LipC6 every other day by IV injection for consecutive two weeks. The peritoneal macrophages prepared from the indicated mice were used to conduct flow cytometry for analyzing the frequency of MIF+MΦ by staining with chromate-conjugated antibodies against for F4/80 and CD74 (MIF receptor).

## Research Project 7: Project Title and Purpose

*Enhancing Smokers' Control over Brain Reward Circuitry Using fMRI Neurofeedback* – Non-drug rewards (e.g., money) are used frequently to enhance the motivation of individuals trying to quit smoking cigarettes. Although this approach is grounded in well-established behavioral principles, converging evidence indicates that non-drug rewards may be least effective at promoting smoking abstinence in the very situations that they are needed most – i.e., when cigarettes are available and cravings are high. The goal of this project is to test the utility of a novel approach for increasing the motivational impact of non-drug rewards in smokers. The project will be used to support a program of research with the potential to significantly improve incentive-based strategies for treating cigarette addiction.

**Duration of Project**

6/1/2013 – 6/30/2014

**Project Overview**

Quitting cigarette smoking and remaining abstinent is notoriously difficult. To bolster their motivation and odds for success, quitting smokers often are advised to reward themselves for maintaining abstinence (e.g., advice posted on the websites for the American Cancer Society and WebMD). More formally, contingency management interventions for the treatment of smoking and other forms of addiction involve reinforcing drug abstinence using tangible incentives (e.g., money). Although the use of non-drug rewards to facilitate smoking cessation is grounded in well-established behavioral principles, converging evidence indicates that non-drug rewards may be least effective at promoting smoking abstinence in the very situations that they are needed most – i.e., when cigarettes are available and cravings are high. Specifically, cues signaling cigarette availability appear to produce a fundamental shift in the sensitivity of motivational brain circuits, rendering them less responsive to non-drug incentives and reducing the degree to which smokers are willing to abstain from smoking in order to earn non-drug rewards. The goal of this project is to test the utility of a novel approach for minimizing the availability-related devaluation of non-drug rewards.

The project will use innovative real-time functional magnetic resonance imaging (fMRI) neurofeedback methods to address the following specific aims: 1) to demonstrate the feasibility of reliably and efficiently isolating reward-related brain regions in individual smokers during fMRI data collection; and 2) to demonstrate the feasibility of using real-time fMRI neurofeedback to train smokers to enhance neural responses to non-drug rewards in brain reward circuitry. Cigarette smokers will be scanned using fMRI while they perform a simple decision-making task during which they earn monetary compensation based upon their performance. The aforementioned real-time neurofeedback procedures will be implemented during the scan session, with the goal of training participants to voluntarily increase reward-related activation in target brain areas.

**Principal Investigator**

Stephen J. Wilson, PhD
Assistant Professor of Psychology
The Pennsylvania State University
140 Ritenour Building
University Park, PA 16802

**Other Participating Researchers**

Joshua M. Smyth, PhD; Charles F. Geier, PhD – employed by Pennsylvania State University

## Expected Research Outcomes and Benefits

This project represents a unique merger of concepts and methods from behavioral addiction research and treatment with cutting-edge methods that analyze and present neural activity in real-time and that recently have emerged from cognitive and affective neuroscience. This rich interdisciplinary approach will be used to test the novel idea that it is possible to train smokers to modulate the activation of specific brain regions using cognitive strategies. We predict that we will be able to rapidly (i.e., within 10 minutes of task performance) and consistently locate core reward-related regions within individual smokers. We also hypothesize that the real-time neurofeedback procedure used in the project will be reliable and robust, such that a significant majority of smokers will acquire self-control over the activation of brain reward regions (i.e., that they will learn to voluntarily enhance reward-related neural activity upon instruction) after a relatively brief period of training (i.e., less than 30 minutes). If the project is successful, it will be used to support a program of research with the potential to have a transformative impact on the design and implementation of incentive-based strategies for treating cigarette addiction. In particular, it will lay the groundwork for identifying the cognitive strategies that are most effective at minimizing/preventing the availability-related devaluation of non-drug rewards and that therefore may serve as a potent adjunct to traditional incentive-based approaches for motivating quitting smokers.

## Summary of Research Completed

Data collection for the project was completed on 6/24/14. The study was conducted at the Penn State Social, Life, & Engineering Sciences Imaging Center. For each participant, a high-resolution, three-dimensional, T1-weighted anatomical image (1.0 x 1.0 x 1.0 mm voxels) was obtained using a magnetization-prepared, rapid acquisition gradient echo pulse sequence (repetition time = 1650 ms, echo time = 2.03 ms, field of view = 256 mm, flip angle = 9°). Functional images were collected using a one-shot echo-planar imaging pulse sequence (38 slices, repetition time = 2000 ms, echo time = 25 ms, field of view = 200 mm, flip angle = 79°). Our goal was to collect usable data from 30 participants. We have been successful in reaching this target. Specifically, data have been obtained from a total of 36 participants (mean age = 23.5 years; 13 male, 23 female), with at least 30 of these participants yielding usable data (preliminary data screening and analysis indicates that we will need to exclude data from 4 participants due to excessive motion during functional magnetic resonance imaging [fMRI] scanning). Thus, we will have sufficient data to address the two specific aims of the project.

The first aim of the study is to demonstrate the feasibility of reliably and efficiently isolating reward-related brain regions within individual participants during functional magnetic resonance imaging (fMRI) data collection. Toward this end, participants completed a monetary reward task while fMRI data were obtained. During the task, participants were required to guess whether the value of a "playing card" was higher or lower than 5, with a monetary gain of $1.00 delivered for each correct guess and a monetary loss of $0.50 delivered for each incorrect guess. Participants were informed that they were playing for real money to be received at the end of the experimental session. Each trial began with a choice-making period lasting 3 sec, during which participants guessed (via button press) whether the value of an upcoming card would be higher or lower than 5 (index and middle finger, respectively). After the choice-making period, a

number from 1 to 9 (excluding 5) was presented for 500 ms, followed by feedback (also presented for 500 ms) informing participants whether or not their guess was correct. Feedback for correct and incorrect guesses consisted of a green upward-pointing arrow (reward trial) and a red downward-pointing arrow (loss trial), respectively.

Unbeknownst to participants, card values were selected only after the response was made for each trial. Task trials were presented in a blocked format, with each block consisting of five pseudorandomly presented trials. Task blocks were separated by 12-second rest periods. Participants performed two types of blocks: 1) *high reward* blocks, comprised of primarily of reward trials (80% correct); and 2) *high loss* blocks, comprised of primarily of loss trials (20% correct). (The inclusion of a small number of incongruent trials in each block was designed to maintain participants' engagement and motivation to perform well.) Participants were not informed about the specific outcome probabilities associated with each block. The task was designed to allow us to isolate regions of interest (ROIs) in a region called the striatum, a brain area strongly implicated in reward-related processing. In order to identify target ROIs in the striatum, Turbo-BrainVoyager software was used to process fMRI data online as they were being acquired during the performance of the monetary feedback task. The data flow for this process consisted of the collection of fMRI images, which then were reconstructed and sent to the scanner console computer, and then transmitted via a high-speed data connection to a computer running Turbo-BrainVoyager (the entire process takes less than 2 seconds). Turbo-BrainVoyager software was used to rapidly preprocess and analyze incoming fMRI data by way of incremental general linear models (GLMs). These incremental GLMs included a predictor for each block condition (high gain and high loss) convolved with a hemodynamic reference function. To isolate target ROIs, Turbo-BrainVoyager was used to compute a contrast of high reward > high loss as the data were transferred in real time. This approach enabled us to localize brain (i.e., striatal) areas that were maximally responsive to nondrug rewards within individuals. Consistent with our objective, we were able to identify ROIs in the striatum for each experimental participant.

In addition to this "on-line" data analysis, we are in the process of conducting "off-line" data analysis using BrainVoyager software. A voxel-wise (i.e., whole-brain) contrast comparing brain activation during high reward and high loss trials revealed that, as predicted, the task was effective at producing activation of the striatum for the sample as a whole. Specifically, as shown in Figure 1, high reward trials were associated with a stronger response in the left and right striatum than low reward trials at the group level. Of primary interest, preliminary "off-line" analyses also further confirm that we were successful in achieving the first aim of the study by effectively isolating ROIs in the striatum at the level of individual participants. Figure 2 presents results from the first three participants. (Off-line data analysis for the remaining participants is ongoing). As shown, we successfully identified ROIs in the left and right striatum for all three participants.

Our second aim was to demonstrate the feasibility of using real-time fMRI neurofeedback to train individuals to upregulate neural responses to non-drug rewards in brain reward circuitry. To achieve this objective, participants completed three neurofeedback training runs after finishing the monetary feedback task described above. During these runs, participants were presented with a "thermometer" comprised of blue and red bars. The height of the thermometer reflected the

strength of fMRI signal from the target ROI identified using the monetary feedback task, such that the thermometer "filled up" with red bars as brain activity in the target area increased and "emptied" to blue bars as activity in the target area decreased. The thermometer was presented on a background that alternated between yellow and green every 20 seconds. During the yellow background, participants relaxed and rested with their eyes open. During the green background, participants attempted to increase the activation of the target ROI by increasing the height of the thermometer. The signal presented via the thermometer was expressed as percent signal change from the estimated baseline in the target ROI and was updated with the acquisition of each functional image (every 2 seconds). Participants were not given overly prescriptive instructions about the specific strategies to use when attempting to upregulate activity in target ROIs (other than instructing them not to think about cigarette-related information). Rather, we suggested that emotional imagery might be useful, but indicated that participants should monitor the feedback signal and "tune" their strategy during successive blocks to determine the most efficient approach for them. This flexible approach was chosen to maximize the likelihood that each participant found an effective strategy. Off-line, raw fMRI data from neurofeedback training runs are being analyzed with BrainVoyager software package using a standard two-level GLM approach, with a focus on contrasting brain activation during "upregulate" and "rest" blocks. We hypothesized that participants would successfully learn to upregulate reward-related neural activity in target ROIs such as the striatum as a result of neurofeedback training. Results from preliminary analyses have provided support for this hypothesis and, more generally, indicate that we were successful in achieving the second aim of the study. Specifically, neurofeedback training was effective at teaching each of the first three participants to increase fMRI activity in the striatal ROIs that were identified using the monetary feedback task, as presented in Figure 3.

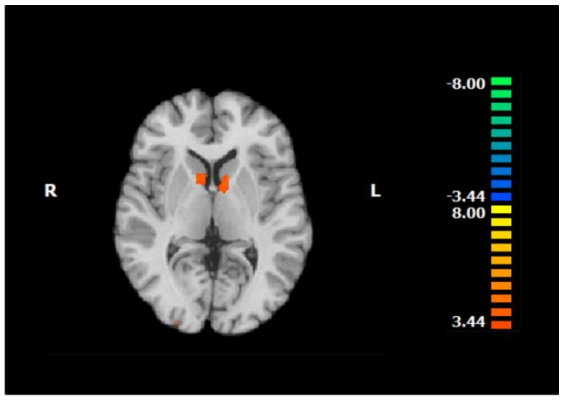


Figure 1. Group-level contrast of high reward versus high loss blocks.

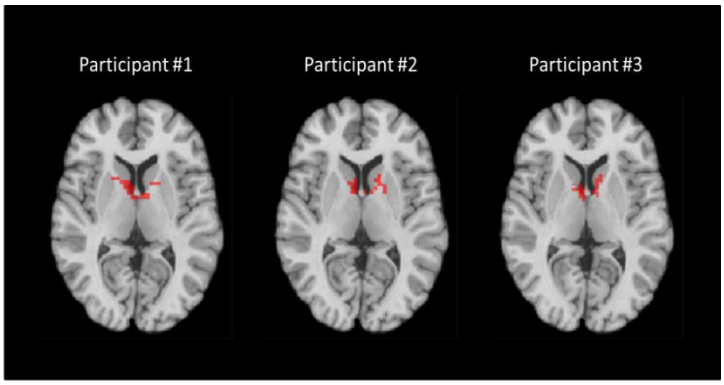


Figure 2. ROIs in the striatum identified in first three participants.

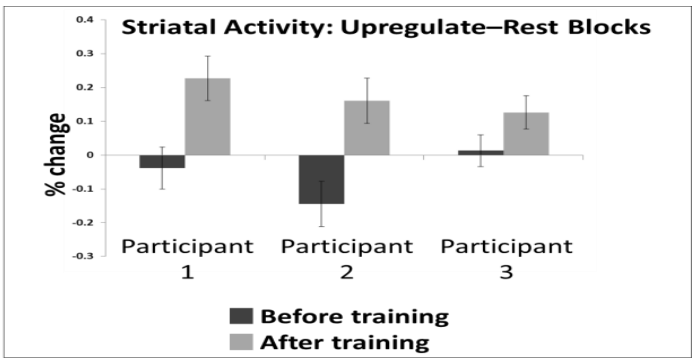


Figure 3. Neurofeedback data for first three participants.

## Research Project 8: Project Title and Purpose

*Mechanism and Inhibition of the Antibiotic Resistance Protein, Cfr* – Cfr is a metalloprotein that employs an unusual reaction mechanism to methylate carbon 8 of adenosine 2503 (A2503) of bacterial rRNA, which leads to resistance to over five classes of antibiotics that target the ribosome. The cfr gene was first identified in 2000 on a plasmid extracted from Staphylococcus sciuri, an animal pathogen. Since then it has crossed over into staphylococci that infect humans, including methicillin-resistant Staphylococcus aureus (MRSA), resulting in a number of fatal infections. More recently, it has been found in Enterococcus faecalis and is widespread in the order Bacillales. Approximately 40% of all clinically used antibiotics target the ribosome. This study aims to generate compounds that will block this reaction as a means of preserving our current arsenal of antibiotics.

### Anticipated Duration of Project

7/1/2013 – 6/30/2015

### Project Overview

The broad objective of this study is to dissect the reaction mechanisms of RlmN and the antibiotic resistance protein, Cfr, and then use the information gained to design molecules that might inhibit these reactions. These two proteins are found almost exclusively in bacteria, and employ very unique reaction mechanisms to catalyze methylation of adenosine 2503 (A2503) in bacterial rRNA. In the case of RlmN, which catalyzes methylation at C2, this methyl modification enhances translational fidelity. In the case of Cfr, which catalyzes methylation at C8, this modification provides resistance to over five classes of clinically used antibiotics that target the ribosome. A key feature of the reaction mechanisms employed by RlmN and Cfr is a protein (RlmN or Cfr)–nucleic acid (rRNA) crosslink intermediate, which must be resolved in the last step of the reaction. Our goal will be to design compounds that will interfere with ribosome assembly by either drastically slowing or preventing the crosslink intermediate from being resolved.

The project has two specific aims.

Aim 1. Synthesize rRNA substrates containing deuterium at C2 and C8 of adenosine, assess the kinetic isotope effect on the reaction, and assess the ability of these compounds to inhibit Cfr or RlmN-dependent methylation in vivo using mass spectrometry. Synthesize rRNA substrates containing fluorine at C2 and C8 of adenosine, and use mass spectrometry to assess whether they elicit formation of an irreversible protein-nucleic acid adduct. Subsequently, assess the ability of these compounds to inhibit Cfr or RlmN-dependent methylation in vivo.

Aim 2. Assess whether antibiotic resistance is elicited solely by C8 methylation of A2503, or whether C2 and C8 dimethylation is required.

**Principal Investigator**

Squire J. Booker, PhD
Professor of Chemistry and of Biochemistry and Molecular Biology
The Pennsylvania State University
302 Chemistry Building
University Park, PA 16802

**Other Participating Researchers**

Tyler L. Grove PhD; Tatiana Laremore, PhD – employed by Pennsylvania State University

**Expected Research Outcomes and Benefits**

The bacterial ribosome is the target of about half of all antibiotics currently in use. The majority of the antibiotics that target the bacterial ribosome bind to its large (50S) subunit, where they can disrupt various functions associated with this complex macromolecular machine, including peptide-bond formation. Bacteria have evolved a number of mechanisms to resist antibiotics that target the ribosome, including modification of the surrounding rRNA. One such modification, methylation of carbon 8 of adenosine 2503 of ribosomal RNA confers resistance against five classes of currently used antibiotics, including phenicols, lincosamides, oxazolidinones, pleuromutilins and streptogramins A and B, as well as the macrolides spiramycin and josamycin. This mechanism of resistance was originally observed in pathogenic species of staphylococcus that infect animals; however, in the last 5 years or so it has crossed over into those that infect humans, including methicillin-resistant Staphylococcus aureus (MRSA) and Enterococcus faecalis. Given that antibiotic resistance in general is growing at an alarming pace, and that humankind is on the verge of entering into an era similar to that before the discovery of penicillin, efforts to combat resistance directly and fervently are needed. The work described herein is geared toward understanding one major mechanism of resistance, with the specific aim of generating compounds that prevent it. It is our hope that these compounds prevent or hinder C8 methylation by Cfr both in vitro and in vivo, and that they can be further developed into practical therapeutics.

**Summary of Research Completed**

*Specific Aim1: Synthesize rRNA substrates containing deuterium at C2 and C8 of adenosine, assess the kinetic isotope effect on the reaction, and assess the ability of these compounds to inhibit Cfr or RlmN-dependent methylation in vivo using mass spectrometry. Synthesize rRNA substrates containing fluorine at C2 and C8 of adenosine, and use mass spectrometry to assess whether they elicit formation of an irreversible protein-nucleic acid adduct. Subsequently, assess the ability of these compounds to inhibit Cfr or RlmN-dependent methylation in vivo.*

We have made considerable progress on this specific aim. Indeed, we have already synthesized a 155-nucleotide (155-mer) strand of RNA containing deuterium at carbons 2 and 8 of all adenines (deu155-mer), and used this RNA to assess whether loss of the C2 hydrogen in RlmN and/or the C8 hydrogen in Cfr takes place in a rate-limiting step of the reaction. *Scheme 1* depicts our

current working hypothesis for the Cfr reaction, wherein loss of the proton is expected to take place in *Step 3* of the mechanism. Last year (before receiving Tobacco Settlement Funds) we published a paper in Nature Chemical Biology that describes the complete characterization of the paramagnetic species formed *after Step 2* of the mechanism by electron paramagnetic resonance (EPR) spectroscopy and other related techniques. Moreover, we showed that the paramagnetic species formed and decayed with rate constants that were consistent with the overall rate of turnover, indicating that it was both chemically and kinetically competent, and therefore likely a true intermediate. In *Step 3* of the mechanism a general base in the active site of the protein is hypothesized to abstract the C8 proton to afford a radical anion. If this mechanism is correct, and if *Step 3* is the rate-limiting step in the reaction, one might expect to observe an isotope effect on the rate of the reaction when deuterium is substituted for hydrogen at C8. We therefore used the deu155-mer RNA substrate that we synthesized and performed rapid-freeze quench EPR spectroscopy to monitor formation and decay of the radical signal.

Shown in Figure 1 (left) are representative EPR spectra obtained in the presence of the deu155-mer substrate. The spectral envelope is consistent with the proposed structure of the radical intermediate as shown in the panel on the right. As can be observed, in the presence of the unlabeled 155-mer, the radical signal accumulates and decays within 3 min of reaction time (black circles in right panel). By contrast, in the presence of the deu155-mer, the radical signal accumulates but does not decay within the 3 min time frame. Spectra on the left indicate that the signal does decay after 15 min, but not fully. This result indicates that there is indeed an isotope effect on loss of the paramagnetic signal, which suggests that loss of the electron from the paramagnetic species and resolution of the enzyme/RNA cross-linked intermediate is gated by proton abstraction. This exciting observation resulted in a fundamental change in the way we viewed the reaction mechanism. Now that we have a coarse view of the kinetics of formation and decay of the paramagnetic species with the deu155-mer substrate, we can better choose the regime in which to obtain appropriate spectra to quantify the intrinsic isotope effect on this step of the reaction.

This isotope effect is also manifested in steady-state turnover reactions. Shown in Figure 2 are Cfr activity assays in the presence of the unlabeled 155-mer substrate or the deu155-mer. In the assay with the unlabeled substrate (Figure 2A), methylation at C8 takes place much faster than methylation of C2. In fact, almost all of the RNA substrate in the assay gets methylated at C8 of A2503 before any of it gets methylated at C2. By contrast, in the presence of the deu155-mer, both the monomethylated (C8 methyl group) and dimethylated species accumulate at the same rate at early time points. The monomethylated species accumulates to approximately the concentration of enzyme in the assay and then stays at that concentration throughout, while the concentration of the dimethylated species continues to increase. At no point is the C2 methylated product observed in the absence of the C8 methyl group. These exciting results suggest that Cfr must methylate C8 before it methylates C2, and that in the presence of the deu155-mer substrate, the kinetic isotope effect on deuterium abstraction is so great that it causes the monomethylated species to accumulate only to the concentration of enzyme present.

Interestingly, RlmN, the protein that catalyzes the C2 methylation of the exact same nucleotide, does not accumulate the cognate paramagnetic species during turnover, suggesting that its rate of formation is slower than its rate of decay. The reaction mechanism in Scheme 1, however,

predicts that if we can identify the base that abstracts the proton from the paramagnetic species, we might succeed in unveiling the radical intermediate, because it would have no mechanism for decay. RlmN and Cfr each contain two cysteines that play intimate roles in their reaction mechanisms. In our original working hypothesis, we proposed that an N-terminal cysteine plays a key role in resolving the protein/RNA cross-link by disulfide-bond formation. However, an alternate role for this cysteine is that in its thiolate form, it could act as the base that abstracts the C2 proton in the RlmN reaction. In RlmN this cysteine is Cys 118. We therefore made C118S and C118A variants of the protein, incubated them under turnover conditions, and analyzed the reactions by EPR spectroscopy. As shown in Figure 3 (left panel), an EPR spectrum was indeed observed with the variant proteins. Appropriate isotopic substitution allowed for complete characterization of the radical species, showing that the predominant spin density was located at N3, although the spin was delocalized about the adenine ring. As shown in the right panel of Figure 3 (blue line), the radical forms but does not decay, which is in contrast to the radical species obtained with Cfr (dashed line). When the cognate variant was made in Cfr (C105S), the radical signal formed but did not decay (red line). These data are consistent with the mechanistic scenario shown in Scheme 1, wherein the base that abstracts the C8 (Cfr) or C2 (RlmN) proton during the mechanism is the second conserved cysteine. These results were recently published in the Journal of the American Chemical Society [*J. Am. Chem. Soc.* (2014) 136, 8221–8228], wherein this Tobacco Settlement Award was acknowledged.

We have also made progress with respect to the second half of Specific Aim 1. We synthesized 2-fluro ATP enzymatically from commercially available 2-fluro-adenosine according to Scheme 2. We then used 2-fluoro ATP in our *in vitro* transcription reactions to generate the 155-mer RNA substrate containing 2F-adenosine at all adenosine nucleotides (2F-155-mer). As expected, RlmN, which acts on the C2 carbon atom, does not convert this substrate into product. Interestingly, however, Cfr, which acts on C8 carbon, does indeed turn this substrate over into product. Shown in Figure 4 are chromatographic traces for assays conducted with RlmN (blue trace) and Cfr (red trace) in the presence of the 2F-155-mer. The black trace corresponds to a control reaction, in which RlmN was incubated with the normal 155-mer substrate. As can be observed, there is a new peak that corresponds to $m^8$2FA, the C8 methylated product of the 2F-adenosine substrate. The intensity of the peak is small compared to the $m^2$A product generated by RlmN with the normal substrate (black trace), suggesting that the fluorine substitution slows the overall reaction. EPR studies to assess what step in the reaction mechanism—formation of the paramagnetic radical intermediate or decay of the paramagnetic radical intermediate—have not yet been conducted.

*Specific Aim 2: Assess whether antibiotic resistance is elicited solely by C8 methylation of A2503, or whether C2 and C8 dimethylation is required*. Previous *in vivo* studies by a group from Denmark indicated that a particular variant of Cfr, Glu91Ala, did not confer antibiotic resistance, although their studies suggested that the protein was modifying A2503 of the rRNA. We engineered this variant and initiated *in vitro* studies of its activity. We found that the variant is particularly unstable, but catalyzes both monomethylation (C8 methylation) and dimethylation of the appropriate substrate, though at a reduced rate (Figure 5). At early time points it appears that monomethylation is significantly faster than dimethylation. Our goal is to use this variant in the background of an *E. coli ΔrlmN* strain, which cannot methylate C2 of A2503, to assess

whether antibiotic resistance is provided by the dimethylated A2503 rather than just C8 methylation.

Scheme 1: Working hypothesis for the reaction catalyzed by Cfr

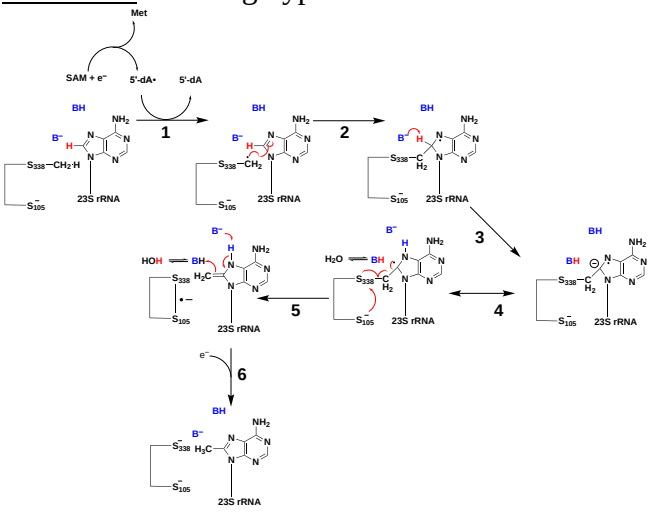


Figure 1. Isotope Effect on decay of radical signal in the Cfr reaction using the deu155-mer RNA substrate. (left) representative spectra at 60 s and 15 min. (right) time course for formation and decay of the radical signal. (black circles) unlabeled 155-mer. (red circles) deu155-mer.

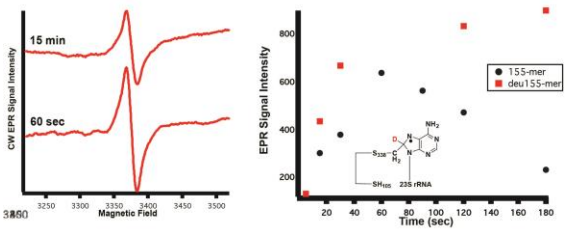


Figure 2. Effect of the deu155-mer substrate on the Cfr reaction. (A) Reaction in the presence of unlabeled 155-mer substrate. (B) Reaction in the presence of the deu155-mer. In both panels the red squares correspond to the monomethylated product and the black circles correspond to the dimethylated product.

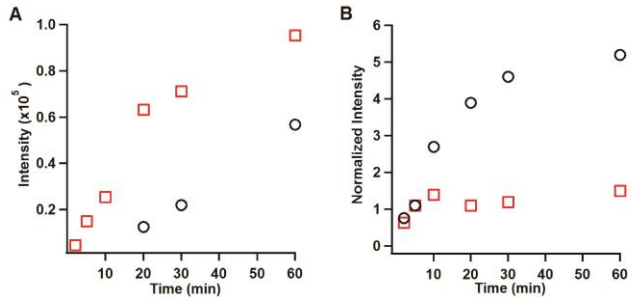

Figure 3. Formation of a paramagnetic signal in an RlmN C118S variant. (left panel) Paramagnetic species in the presence of unlabeled 155-mer (not labeled); deu155-mer ([$^{2}$H]); deu155-mer with $^{13}$C-labeled methylcysteine residue ([$^{2}$H, $^{13}$C]); and unlabeled 155-mer with $^{13}$C-labeled methylcysteine residue ([$^{13}$C]).

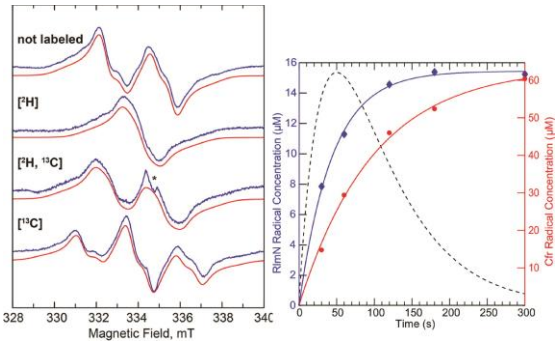


Scheme 2: Synthesis of 2-fluro-ATP from commercially available 2-fluro-adenosine.

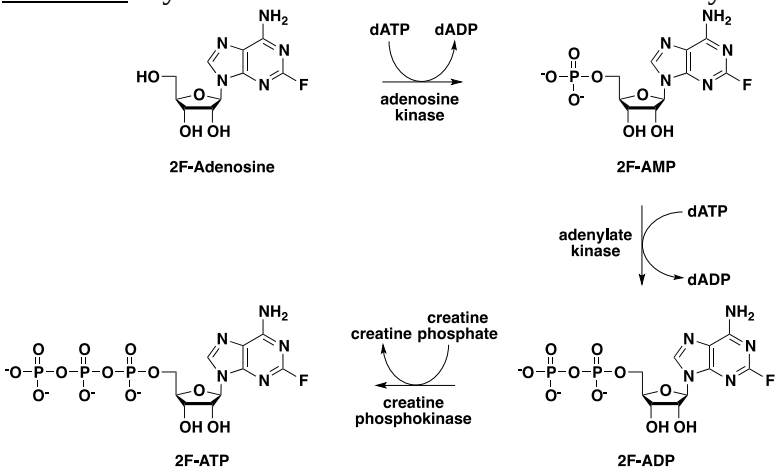


Figure 4. Effect of the 2F-155-mer on turnover by RlmN and Cfr. Black trace is RlmN reaction with normal 155-mer substrate; blue trace is RlmN reaction with 2F-155-mer substrate; red trace is Cfr reaction with 2F-155-mer substrate.

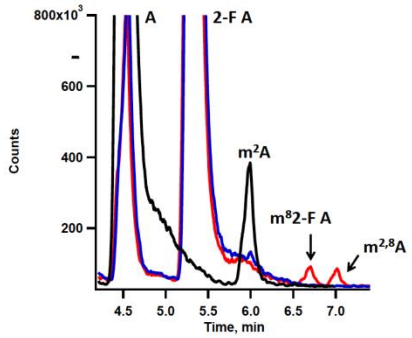

Figure 5. Turnover of Cfr Glu91Ala variant. Green squares correspond to monomethylated (C8) product, while black squares correspond to dimethylated product.

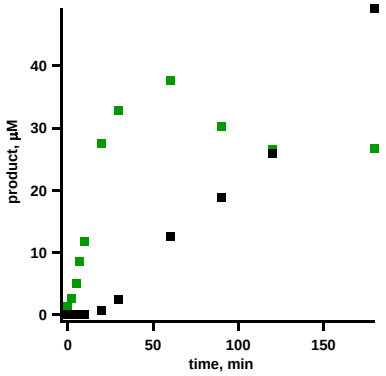


## Research Project 9: Project Title and Purpose

*Research Infrastructure: Zebrafish Functional Genomics Core* - The project will renovate existing animal facilities to build a new Zebrafish Functional Genomics Core for Penn State scientists and collaborators to develop zebrafish as a vertebrate model for human disease. The research resource can be used by scientists interested in using a powerful vertebrate model system, the zebrafish, to study human biology and disease.

### Anticipated Duration of Project

2/28/2014 - 6/30/2016

### Project Overview

The project's goal is to modernize, expand, and consolidate our current zebrafish capabilities through the creation of a Zebrafish Functional Genomics Core (ZFGC).

Our first aim will be to increase and centralize housing space, quarantine space, and procedural space through renovation of four existing, underutilized animal rooms totaling over 1,200 net square feet. Aging and dispersed facilities would be consolidated to a central, better-monitored, commercial-grade system, in combination with an adjacent zebrafish procedure room that includes equipment for microinjection, mass breeding, and photography, and additional quarantine space. This arrangement will improve efficiency of workflow, result in cost savings for investigators by pooling of time, labor, and space requirements, and at the same time promote interactions among researchers. Dedicated water filtration and treatment will result in standardization of housing conditions across the fish populations. The purchase and installation of a new multi-rack zebrafish and bio-filtration and aeration system will be supported by a reverse osmosis water system similar to systems successfully operated for nearly 18 years. The amount of space allocated to zebrafish in the Central Animal Quarters (CAQ) increases 162% from 474 net sq. ft. to a total of 1,242 net square feet. The centralized core facility will house all of the fish in one location. The new facility includes space for future expansion of fish

housing to meet anticipated growth in zebrafish research.

Our second aim will be to improve the efficiency and cost-effectiveness of the care and use of zebrafish through the installation of a state-of-the art zebrafish husbandry system. This system requires specific equipment and will require us to develop standards of practice in the environmental, molecular, cellular and practical aspects of using zebrafish (e.g. habitat preferences, diet and feeding, health, breeding, disease prevention). The development and refinement of all aspects of animal husbandry are critical for the scientific, ethical, and animal welfare concerns within the context of an efficient and cost-effective laboratory.
Our third aim will be to establish a dedicated procedure room for shared operations including microinjection, mass breeding, the study of mutant and morphant phenotypes, and photographic documentation of results that will serve as the location for experimental execution and hands-on instruction. Execution of this aim will require installation and use of microinjection machines, vacuum pumps, microscopes with ergonomically adjustable headpieces, digital cameras, and computers for digital photographic software and for design of morpholinos and primers for gene editing.

**Principal Investigator**

Keith C. Cheng, MD, PhD
Penn State Hershey College of Medicine
Division of Experimental Pathology
Jake Gittlen Cancer Research Foundation
500 University Drive Rm C7866A
Hershey, PA 17033

**Other Participating Researchers**

Glenn Gerhard, MD – employed by Pennsylvania State University College of Medicine

**Expected Research Outcomes and Benefits**

The zebrafish has shown explosive growth in its use as a model system. It's exquisite transparency allows direct observation of transgenically fluorescent cells. Expression patterns can be determined for specific genes using whole-mount hybridization. Zebrafish is now the most commonly used vertebrate for genetic screens. This core will have high impact, because it will enrich and connect three of our new and growing institutional health research investments: The Institute for Personalized Medicine, the Drug Discovery Development and Delivery Core (D4), and a university-wide Systems Biology cluster hire.

Accomplishing these aims will facilitate the use of zebrafish in currently funded projects involving human cancer, cardiovascular disease, metabolic disorders, neurodevelopment and skin pigmentation. A pilot project program using other funds will ensure lasting use of this new core, as well as integration of research activities between cores. Newly targeted directions of research utilizing the zebrafish model will include personalized medicine, disease modeling, and drug discovery.

**Summary of Research Completed**

Milestone for reporting period for 2/28/2014 -6/30/2014: Begin construction, hire Core personnel, and purchase necessary equipment for core.

During the initial 3 months, the construction committee made modifications to the design of the Zebrafish Core. After a review of the original plan to increase core capacity in phases, it was decided instead to maximize housing capacity at the outset to avoid construction-associated disruption of multiple research programs. Review of the core design led to the realization that we had to upgrade the filtration system. The increase in system capacity resulted in additional costs of $421,010, bringing the new total to $1,263,727. Since the G20 ($476,191) was awarded in 2013, construction and equipment costs have increased to $1,263,727, and the costs of staffing and maintenance bring the total project cost to $1,886,342. CURE funds total $356,550 with the balance being Departmental match.

The modified plans were submitted to NIH for approval. We received NIH approval of the amended plans for construction and opened the project for bidding. Dr. Khai Chung Ang was hired as our Ph.D. level scientific director. Sarah Arnold-Croop was hired as our Chief technical director. The PI and Ms. Arnold-Croop attended two zebrafish meetings to update knowledge of technologies and to acquire information about how other zebrafish cores are run across the country.

We have been actively recruiting investigators from University Park and Hershey to use zebrafish as animal model. Co-director Glenn Gerhard and also Dr. Nelson Yee in the Cancer Institute are using zebrafish. Neuroscientist and neurologist Mark Stahl, MD, PhD, who uses zebrafish as his primary model organism, was successfully recruited and will join our faculty in August 2014, in large part based on the anticipated access to the ZFGC. This recruitment is particularly important since the most common organ system affected by gene knockouts and chemical toxins may be the nervous system. Dr. Cheng just met with Dr. Raymond Huhl, Director of the Penn State Cancer Institute, and is meeting with a group that includes members of the departments of Pediatrics and Neurology within the week to develop further collaborations.

The ZFGC's potential positive impact on Penn State is already enhanced by its connections with other institutional health research investments including The Institute for Personalized Medicine, Cancer Institute, the Drug Discovery Development and Delivery Core (D4), and a university-wide Systems Biology cluster hire initiative.